CERN-PRE-78-092

CERN LIBRARIES, GENEVA

CM-P00063969

ZATION FOR NUCLEAR RESEARCH

A LARGE LIQUID-ARGON SHOWER DETECTOR FOR AN ISR EXPERIMENT

J.H. Cobb, S. Iwata*), D.C. Rahm, P. Rehak and I. Stumer

Brookhaven National Laboratory, Upton, New York, USA

C.W. Fabjan, M. Harris, J. Lindsay, I. Mannelli**), K. Nakamura***), A. Nappi**), W. Struczinski†) and W.J. Willis

CERN, Geneva, Switzerland

C. Kourkoumelis††) and A.J. Lankford†††)

Yale University, New Haven, Connecticut, USA

Geneva - 7 June 1978

(Submitted to Nuclear Instruments and Methods)

---

*) Permanent address: Nagoya University, Nagoya, Japan.

**) On leave of absence from the University of Pisa and the Istituto Nazionale di Fisica Nucleare, Sezione di Pisa, Italy.

***) Permanent address: University of Tokyo, Tokyo, Japan.

†) Now at the Physikalisches Institut, Technische Hochschule Aachen, Germany.

††) Now at the University of Athens, Greece.

†††) Now at the University of California, Berkeley, Calif., USA.

ABSTRACT

A large liquid-argon shower detector system has been constructed for the detection of photons and electrons at the CERN ISR.

The calorimeter system is built in a modular way such that eight modules would cover $\phi = 2\pi$ azimuthally with a total solid angle of $\Omega = 8$ sr. Each module consists of 1.5 mm thick lead plates, spaced 2 mm apart. Longitudinal grouping and transversal division into strip-like sections of the charge-collecting electrodes provide the required spatial resolution and hadron discrimination.

Measurements on energy and space resolution and electron/hadron discrimination are described. The signal-processing system, designed to minimize electronics noise, can handle event rates up to 0.5 MHz and provides energy information for trigger purposes.

The performance of this calorimeter system during two years of ISR operation is reported.

1. INTRODUCTION

This paper presents a description of a calorimeter built to record electromagnetic showers from electrons and photons produced at the CERN Intersecting Storage Rings (ISR). This apparatus utilized the principle of a sampling ionization chamber with liquid argon (LA) as the active medium, a technique which we have developed in several prototypes. Many fundamentals of the technique were tested in those prototypes and have been described in our previous papers[1-3].

Here we will describe the features of the detector which were required for an experiment aimed at the detection of electron pairs produced in pp interactions at the ISR[4]. This is a process with a small rate and potentially large background. A detector with the following properties was required:

i) capability of covering the full solid angle with a minimum of dead area;

ii) very good electron/hadron discrimination;

iii) good energy resolution for electrons and photons;

iv) good position resolution;

v) ability to handle rates up to $\sim$ 1 MHz;

vi) ability to provide very selective triggers;

vii) stable operation over long periods.

The electron/hadron discrimination was obtained by observing the characteristic shape of the electromagnetic and hadronic shower in the transverse and longitudinal direction, as well as by a novel transition radiation detector, which is described in detail elsewhere[5,6]. A LA ionization calorimeter allows great freedom in subdividing the detector volume in order to observe the shape of the shower in three dimensions. The sensitivity of all sections was kept equal by stable and absolute charge calibration, making it possible to build a large system without deteriorating the energy resolution. Only one over-all constant must then be determined in order to translate charge measurement to energy.

Figure 1 shows a cross-section through the experiment in the ISR. The detectors are modular, such that eight modules could be packed closely and give nearly full azimuthal coverage. At present, only four modules have been built, and these have been run in several configurations to cover different azimuthal regions.

Subdividing the calorimeter volume into strips, oriented in different directions, gave transverse resolution of about 10 mm as well as longitudinal subdivision into three regions. The good position resolution ensures that a shower can be reliably correlated with a charged track observed in the proportional wire chambers. Also, neutral pions with one photon converted to electron pairs will still usually be recognizable as two showers with the effective mass of a pion, giving control over an important background in searching for direct electron production.

Another goal of the experiment was to measure photons from π's, η's, χ-decays, or directly produced photons, etc. In general, the specifications for an electron detector are compatible with this function, but if this had been the sole goal, less emphasis would have been put on hadron rejection and more on high efficiency in the pattern recognition of several photons within a small cone of angles.

The layout of the strips is shown in Fig. 2. They provide four different projections of each shower and a longitudinal subdivision of the shower into three regions.

2. MECHANICAL DESIGN OF THE CALORIMETER TANKS AND ABSORBER STACKS

An artist's view of one of the calorimeter tanks is shown in Fig. 3. Each tank is made of a high-strength aluminium alloy (SB 209-5083 H-111) and is designed to be operated at pressures up to 1.3 bar above atmospheric pressure[7]. The entrance window, at a radial distance of approximately 76 cm from the ISR beams, is 20 mm thick and covers an area of 65 × 190 cm^2. The backplate, at a radius of $\sim$ 115 cm, has the dimensions 95 × 190 cm^2. We preferred to construct the tanks from this aluminium alloy rather than from stainless steel for two reasons: firstly to minimize the material on the particle path before reaching the active absorber stacks; secondly, the much larger thermal conductivity of Al facilitates the uniform cool-down of the tanks and minimizes the danger of local "hot spots". Cryogenic connections for the circulation of the LA are made at the side faces of the tanks through four standard-size flanges (32 mm inner diameter) on each side. These flanges are made from stainless steel to match the material of the cryogenic plumbing and are welded to the Al body with a SS-Al explosion-bonded

transition piece*). Electrical connections to the absorber stacks are made via feedthroughs, which remain helium-leak-tight at LA temperatures (∿ 80 K). Signal processing required two different types of feedthrough. One, ∿ 30 mm in diameter, provides 37 pins, insulated in sintered glass powder**). Six such feedthroughs are used per tank for 96 signal channels. A larger feedthrough**), custom made, was required for 16 signal channels, transmitted via flat ribbon cables (Fig. 4).

The tanks equipped with the absorber stacks weigh approximately 2 tons. They are supported from the end faces (Fig. 5). Two sets of pins are bolted to each of the sides, spaced with 10 mm thick, glass-fibre-reinforced epoxy resin washers to reduce heat losses. Arms in sliding mounts connect to external support structures, and extend inwards for the support of other detector elements.

A cross-section through such a tank is given in Fig. 6, showing the layout and the mounting of the absorber stacks. In depth the absorber volume is subdivided mechanically into five "shelves"; the absorber plates of each shelf are supported by aluminium plates (8 to 10 mm thick); these in turn are bolted to the slanted side walls of the tank, providing an additional stiffening element for the tank.

A schematic diagram of the electrode disposition was given in Fig. 2. The innermost stack has signal electrodes in the direction of the ISR beams, 20 mm wide, providing azimuthal information of the particle direction (ϕ strips). In the second shelf, the signal electrodes (again 20 mm wide) are inclined alternately at $\pm 20^\circ$ to provide two more stereo views; additional coarse information on the polar coordinate is obtained from shelves 3, 4, and 5, with 100 mm wide signal electrodes perpendicular to the ϕ strips. In all shelves, the ground plates were made from 1.5 mm lead sheets; the signal electrodes of the small strips were machined into a copper/glass-fibre sandwich [0.5 mm copper glued to the two sides of a 1 mm thick glass-fibre epoxy resin sheet***)]. A summary of various properties of the absorber stacks is given in Table 1.

---

*) Manufactured by EF Industries, Boulder, Colorado, USA.

**) Manufactured by SETA S.A., Ets. C. Doloy, Paris, France.

***) The Cu/glass-fibre epoxy sandwich was manufactured by Stesalit A.G., Zullwill, Switzerland.

The absorber stacks are thus made of sheets of lead and copper with spacers between the sheets determining the thickness of the liquid-argon gap. The ionization produced in the LA gap is collected, and it is this signal that gives the energy information. The total thickness of the LA gap has to be known to 1%, while a slight variation in the individual gap widths is tolerable.

The spacers used between the plates should introduce a minimum of dead area to minimize effects on the performance of the detector. In our apparatus the design of spacing elements is determined by the mechanical properties of lead. The choice of an absorber material with high atomic number Z is an advantage when differences in the longitudinal development of electromagnetic and hadronic showers are used to discriminate between the two kinds of particles. The ideal material is tungsten, but costs and machining properties exclude its large-scale use. Uranium is an attractive possibility, which also allows the construction of very compact detectors. We choose "dispersion-strengthened lead", a lead alloy containing about 1% PbO *). This alloy has a tensile strength comparable to an 8% antimonial lead, but has a factor of 3 higher creep resistance. These mechanical properties permitted us to ensure the spacing between ground and signal planes with 5×10 mm^2 glass-fibre epoxy resin washers of the nominal gap thickness distributed on an $\sim 15 \times 15$ cm^2 grid. These spacers were glued onto the lead sheets with epoxy glue (Araldite). A second requirement was imposed by the different coefficients of thermal contraction of the materials used. The lead plates had therefore to be mounted so that they could slip with respect to the Al support-plate. This was achieved by making outsize holes in the lead plates for 18 glass-fibre epoxy resin screws which supported and anchored the stack to the aluminium plate. Glass-fibre epoxy resin washers maintained the gap spacing. The support screws were carefully tightened to a tension which still permitted sliding of the sandwich plates relative to each other. Tests and operational experience have shown that this construction permits satisfactory operation over long times and many (> 20) cooling cycles, provided the cool-down operation is carried out slowly and carefully.

---

*) Manufactured by Associated Lead Manufacturers, Ltd., Chester, UK.

The mechanical design concept of the calorimeters described here was adopted with the aim of constructing detectors, which could, if necessary, be rapidly and conveniently repaired. Easy access to the absorber stacks is ensured by the demountable backplate. The subdivision of the absorber volume into five independent units facilitates mechanical and electrical assembly. The support method for the detector plates permitted final designs with a minimum of large-scale testing. This simplicity in the construction, however, adversely affects the performance of the detector in two ways: the Al support-plates provide enough dead volume (Table 2) to influence the energy resolution of the device; secondly, the same electrical and mechanical grouping provides for easy cabling but with decreased efficiency in the off-line pattern recognition of the showers. A fully optimized construction would avoid having to use the intermediate support-plates. One could also give more consideration to interleaving the various directions of the signal electrodes. This would permit using pulse-height matching to resolve certain ambiguities in the pattern recognition.

3. CRYOGENICS

As explained in the Introduction, we required a modular system with units which could be assembled in a compact array. Since an individual module can be mounted at any angle with respect to the vertical, a gas-liquid interface was not allowed. To ensure that each tank is completely filled with liquid, the LA it contains must be maintained at a pressure higher than the vapour pressure of LA at the temperature of the tank. We considered the alternatives of cooling the tank by means of a heat exchanger mounted on it or in it, or circulating LA between the detector tank and an external heat exchanger by means of a pump. We chose the latter method because no additional equipment needs to be mounted on the detector tanks, and because identical properties of the LA in each tank are ensured by the mixing in the heat exchanger. (The method of using a LN_2 heat exchanger coil mounted on the surfaces of a tank was tested on one of our completed units and found to work satisfactorily. This method has an advantage in that the pressure fluctuations which tend to occur in the circulating fluid are isolated

from the detector and its relatively fragile entrance window. The cool-down was much simpler and the consumption of LN_2 should be much less.)

A simplified flow diagram is shown in Fig. 7. The heat exchanger is used also as a storage vessel for the LA. The temperature of this vessel is maintained by controlling the flow of LN_2 in a heat exchanger mounted at the top, so that the LA vapour pressure is kept at 0.3 ± 0.1 atm. The LA is withdrawn from the bottom of this vessel to the inlet of a centrifugal pump which produces a pressure of 1.5 atm at a flow rate of about 2 ℓ/sec. This liquid then passes through a heat exchanger which transfers the heat introduced by the pump back to the LA in the storage vessel. The LA then is brought to the detector through flexible, vacuum-insulated lines and returned in the same way to the storage vessel. The heat flowing into the detector tanks increases the temperature of the returning liquid by less than one degree, and the overpressure maintained by the pump is such that the LA in the detector tanks does not boil.

The cool-down requires about two days and is limited by the available rate of heat transfer from LN_2 to the LA storage dewar. Very small amounts of liquid are admitted to the detector by remotely operated pneumatic valves. The temperature of the detector modules is monitored with thermocouple measurements. When the modules reach LA temperature they start to fill, and the valve controlling the LA flow may be fully opened.

The detector tanks are insulated with polyvinylchloride foam*), 5 cm thick on the entrance face and 15 cm thick on the other faces. The heat load is about 0.5 kW, with about one third due to the electrical leads and their surroundings. Comparable heat loads were encountered in the pump, the piping, and the 60 m long LN_2 filling line (and, when in use, the argon purifier), requiring about 5000 ℓ/day to operate the whole system. A system with much lower heat loads could be built, but the required investment was not considered justified for an installation that was expected to be used only for a short time, and which had to be built quickly and with flexibility of rearrangements. Heating elements are placed on the box

*) "Klegecell", manufactured by Kléber-Renolit Plastiques, Lyon, Mouche, France.

containing the preamplifiers and on a thin (1 mm) aluminium plate on the exterior of the entrance face of the detector, and are regulated to keep these points at ambient temperature.

An extensive safety system was installed. Overpressure protection is provided by

i) solenoid valves, which open fully to the vent when the overpressure exceeds 1.0 atm;

ii) conventional pressure relief valves set at 1.2 atm;

iii) rupture disks designed for 1.4 atm.

The vent line is a 40 cm diameter light-weight duct leading outside the ISR tunnel.

The purity of the LA was established by measuring the O_2 content of gas obtained from liquid boiling in a line from the pump exit. A commercial O_2 analyser with an accuracy of 0.1 ppm was used. When the O_2 content exceeded about 1 ppm, usually owing to an incorrect flushing operation, a purifier was used, taking gas from the pump exit and returning it to the storage vessel[2]). On one occasion, an O_2 content of several ppm was found after filling. Use of the purifier removed the O_2, but the response of the detector to photons and to minimum ionizing particles showed that some other impurity was present, reducing the charge collected by about 30%. As a rule, periods of steady operation of several months showed no appreciable change in purity. This is illustrated in Fig. 8, which shows the value of the π^0 mass obtained using the nominal calibration over such a period of time.

4. ELECTRONICS

The intended application of this equipment required the detection of showers with energies down to a few hundred MeV. The longitudinal subdivision needed for electron identification leads to shower fluctuations, which can result in small energy deposits in a given layer even for GeV showers. Consequently, it was required that the noise levels be below the signal due to a minimum ionizing particle. This is feasible, using a 2.0 mm LA gap, if extraneous sources of noise are avoided,

so that the theoretical minimum of noise is achieved. The theory, and some of the practical steps necessary to obtain the theoretical values, are detailed in previous publications[1,8]. Here it may be useful to describe the methods used to derive a trigger from the calorimeter signals, and the considerations that arose in building and operating a system with a large number of channels.

Figure 9 shows a block diagram of the electronics. One of the most critical parts was the connection between the individual electrodes and the preamplifier. The high-rate environment of the ISR required that the total length of the signal had to be kept to a minimum. Noise considerations and mechanical design fixed the smallest allowable gap at 2 mm, and the corresponding electron collection time is then about 300 nsec. The inductance allowed in the connections and the leakage inductance in the input transformer were then determined by[1]

$$L << \frac{\lambda^2}{64\ \pi^2\ C_d}\left(1 + \frac{C_d}{C_b}\right)\left[1 + \left(\frac{n}{n_{opt}}\right)^2\right]\frac{n_{opt}^2}{n^2}\ ,$$

where λ is the length of the shaped pulse, C_d is the detector capacitance, C_b is the high-voltage blocking capacitance (in units of μF), n is the input transformer turns ratio, and n_{opt} is the turns ratio for minimum noise. The best compromise between noise and inductance limitation is $n \simeq 0.6\ n_{opt}$ [1]. For our conditions

$$L << \frac{1.42}{C_d} \times 10^{-14}\ .$$

Our cables are 1 m long. The inductance of such a cable, with impedance Z_0 (Ω) and with a Kapton dielectric, is $L \simeq 7 \times 10^{-9}\ Z_0$. Thus we must fix the cable impedance such that

$$Z_0 << \frac{2.84 \times 10^{-6}}{C_d}\ .$$

The length of cables from the end of the stack to the preamplifier was about 1 m. The capacitance of the ϕ, u, v strips leads to an allowable inductance consistent with the use of twisted-pair cables. The larger capacitance of the θ blocks required the use of strip cables of 4 Ω impedance. Similarly, the use of

standard pin-type feedthroughs was permissible for the passage of the twisted-pair cables through the wall of the LA tank, while the strip cables needed the specially designed low-inductance feedthrough shown in Fig. 4. This had pairs of metal strips spaced by 1 mm and sealed in glass. The strip cables were connected to the feedthrough by means of a standard two-sided printed circuit connector. The same method was used to connect at the detector and preamplifier card ends.

We required a minimum of dead space at the sides of the detector, so that two units could be placed close to each other; therefore the read-out had to be entirely at one end. However, half the u, v strips terminate at the other end of the detector, and the θ blocks are accessible only from the sides. In both these cases the problem was solved by fabricating thin, low-inductance, strip connections on printed circuit boards, which were inserted into the body of the detector as one layer of electrodes. In the case of the u, v strips, these boards provided 32 pairs of strip cable running the length of the detector, bringing the signal to the read-out end. For the θ blocks, the signal from the block was connected to the strip cables at the sides of the detector where the blocks were accessible, and conveyed to the read-out end.

Within a given layer there were low-inductance buses to place the strips in parallel. These were connected to individual electrodes with 1.5 mm × 0.2 mm copper strips, about 10 mm long, bent into an "S" shape to provide for contraction at low temperature. These were soldered into 0.5 mm wide slots cut into the lead strips.

The high voltage was distributed to each detector element through a 1 MΩ resistor. A short circuit in one element did not affect the others. Most short circuits were apparently due to small slivers of lead from the plates. These could usually be removed by discharging a capacitor through the external connection. Before special potted capacitors*) were installed on the θ blocks, a number of blocking capacitors developed short circuits. These detector elements were temporarily restored to service by installing an external blocking capacitor, and

---

*) Manufactured by Custom Electronics, Oneonta, NY, USA.

running the element at a lower voltage consistent with the voltage holding capacity of the feedthrough.

The calibration signals for the strips were introduced on the preamplifier cards through accurately adjusted capacitors. This method was not adequate for the θ blocks, because despite the use of the low-impedance cables, the inductance would have distorted the pulse shape to such an extent that the charge calibration would not have been accurate to the 0.5% specified. Also, the ratio of blocking capacitance to detector capacitance was only 4:1 and in this case the variation in these capacitors would affect the calibration. Therefore, the calibration signals for the θ blocks were introduced directly on the detectors, in the LA. For the calibration signals a pulser in the counting room was used which generated voltage steps with an accuracy of 0.01%. These were routed through a switching box by means of reed relays to the individual detector elements of the modules. At the detector they were applied to a network which had the correct terminating impedance to produce a signal with the same rise-time as that due to the electron collection. This avoided calibration errors due to varying ballistic deficits from different lead inductance in different channels, and kept a correct absolute charge calibration*). The calibration capacitors in the LA were made of Teflon-based printed circuit board, and the capacitance of each one was measured and corrected for the 4% increase at LA temperature. These devices were carefully shielded to allow a precise three-terminal measurement of the true calibration capacitance and to prevent cross-talk.

Cross-talk in the input connections and the feedthrough was found not to be a problem, especially since the input of the charge-sensitive amplifiers is nominally a null point in the feedback loop. Cross-talk in the output is a more serious problem. The first unit constructed had a single-ended drive, and suffered from unacceptable cross-coupling in the preamplifier box as well as in the 60 m twisted-pair cable. This was corrected by introducing the balanced drive shown in Fig. 9. The shaping amplifiers receive this signal differentially, resulting

*) See Fig. 2 of Ref. 2.

in a low cross-talk and great insensitivity to common mode pick-up. The shaping amplifier was similar to that used in previous work except for a slightly longer shaping time to render the system less sensitive to lead inductance, and the use of multi-transistor chips and a more compact layout in order to place eight channels in a CAMAC-style module.

The shaping amplifier was used to form and distribute the sum-signals which in turn were used in the trigger; this trigger was needed in order to select single electrons and photons above a certain energy. The electromagnetic character of the showers was determined by the longitudinal subdivision of our detector, but if all the electromagnetic energy in one module, covering 1 sr, were summed, this trigger would have preferentially selected events with a number of low-energy photons and electrons. For this reason a localized energy deposit was obtained by summing over four ϕ strips or five u or v strips, as shown in Fig. 10a.

In order to avoid edge effects, sets of overlapping sums are formed to ensure that at least one sum will exceed the discriminator threshold for the desired showers.

Since the primary trigger in the experiment is based on the signals from these detectors, the signals have to be delayed until the trigger decision can be made and gates distributed to the analog-to-digital converters (ADC) which record the signal for each section in the calorimeters. This relative delay is achieved by a combination of two measures. There is a miniature lumped delay line of 100 nsec introduced in each channel in the shaping amplifier output. Also the sum used for the primary trigger is made using the derivative of the localized energy sums, thus advancing the sum-signal with respect to the normal output by 150 nsec. The undifferentiated sum, which has lower noise, is also made available for use in second-level trigger conditions, which are evaluated after the ADC read-out has been initiated.

The sum-signals involved contributions from a number of different shaping amplifier modules. This was achieved by using the buses on the rear of a CAMAC-style crate. Individual modules inject current signals to the summing buses. Special modules in the crate receive the sums for threshold discrimination and

buffer the analog signals for further distribution. All input signals were wired to the rear connector, so that the only connection made on the front panel of the shaping amplifier modules was the multiconductor connector leading to the ADC.

For the off-line analysis, a gain calibration is made using 100 successive calibration pulses at the start of each tape. These calibrations of the whole system were usually found to remain stable to 0.5% for months, unless a module was exchanged for repair. Besides the frequent gain monitoring for use in the off-line data analysis, the electronics gains of the linear channels were individually adjusted and kept to within ±5% of the nominal value, in order to minimize the effect of gain variations on the trigger threshold.

5. PERFORMANCE OF THE CALORIMETERS

5.1 Beam tests

The performance of these devices was investigated in several exposures to electron and hadron beams of known momenta.

In Fig. 11 we show the measured signal as a function of incident electron momentum. The response is linear to $\lesssim 1\%$ in the measured range 0.75 GeV/c to 4 GeV/c. The pulse-height distributions are shown in Fig. 12. The measured resolution as a function of energy can be parametrized in this form:

$$\frac{\sigma(E)}{E} \approx \frac{0.10}{\sqrt{E}} , \quad \text{with E in GeV .}$$

The resolution is somewhat worse than the one expected from Monte Carlo calculations for comparable sampling geometries and when compared with measurements carried out by us on a small device but with similar plate structure, which gave $\sigma(E)/E = 0.08/\sqrt{E}$. Similar conclusions are derived from other measurements on sampling devices with different materials and geometries of absorber plates[2,9]. All these results can be parametrized in a form

$$\frac{\sigma(E)}{E} \simeq 0.05 \left[\frac{d\varepsilon}{dx}\right]^{1/2} \frac{1}{\sqrt{E}} ,$$

where $d\varepsilon/dx$ is the ionization loss in MeV per sampling cell for a minimum ionizing particle[1] (however, see Ref. 10). We attribute this loss of resolution in the

large detector to the various dead zones, particularly the support structures, as indicated in Section 2.

It is interesting to compare the average total collected charge with predictions. Naively one would expect

$$Q = E \frac{Q_e}{2\phi_{LA}} \frac{dE/dx \text{ (sensitive gap)}}{dE/dx \text{ (sampling cell)}} ,$$

where

E is the energy deposited by the particle in the calorimeter (= ionization loss for muons, total energy for electrons);

Q_e is the electron charge = 1.6×10^{-19} Coulomb;

ϕ_{LA} is the measured ionization potential for LA [10] = 24 eV.

Repeated measurements carried out by us on this and other detectors with different geometries and materials[1,2] (Fe, U) show that the collected charge is consistent with the naive prediction for muons, but is typically and rather universally only about 70% of it for electrons. This is not a property of the LA, as a similar ratio has been measured in a uranium/scintillator sampling calorimeter[12]. We believe that it might be explained by "transition effects" between the boundaries of the active and passive absorber layers, which influence, in particular, the last, very low-energy generation in the electromagnetic shower and which causes a disproportionate energy loss in the higher density passive absorber*).

The narrow-strip electrodes permit rather precise localization of electromagnetic showers, which precision is only weakly dependent on energy. In Fig. 13 we show the distribution of the centres of gravity of the showers with respect to the position of the incident electrons, indicating a spatial resolution of

$$\Delta x \simeq 5 \text{ mm} .$$

We investigated the longitudinal and radial development for electron- and pion-induced showers. The differences in the respective longitudinal development are used to define those conditions which at the trigger stage discriminate most

*) A recent, detailed Monte Carlo study of electromagnetic shower development reproduced rather well the observed e/μ ratio: C.D. Orth, private communication.

efficiently between electrons and hadrons. For this purpose, cuts are applied to the energy deposited in the first $\sim$ 3 radiation lengths (the ϕ shelf) and also to the energy in the second shelf (u + v). As an example of these measurements, we show in Fig. 14 the results for 4 GeV electrons and pions. Iso-efficiency curves can be constructed for electrons as a function of the energy cuts in the ϕ and (u + v) shelves. The corresponding pion acceptances are also indicated. Based on the ratio of the energy deposits in the two layers, pion rejections of $\gtrsim 10^2$ are achieved.

The differences in longitudinal shower development are strikingly displayed in several scatter plots. Figure 15 shows for 4 GeV/c electrons the correlation between the charge in the ϕ shelf, $Q(\phi)$, versus the energy deposited in (u + v), Q(u + v). For electrons, a strong correlation is observed, with an energy deposit Q(u + v) proportional, on the average, to $Q(\phi)$. For pions however (Fig. 16), the correlations are much smaller.

The different nature of electromagnetic and hadronic showers is shown in another way in Fig. 17 (electrons) and Fig. 18 (π^-) where we show the differences in Q(u) - Q(v) as a function of the energy deposited in (u + v). The quantity Q(u) - Q(v) measures the fluctuations in the shower development; it is much larger for π^-'s, which is characteristic of hadronic showers. Additional information, which helps in the discrimination of e/π, is provided by an estimate of the radial shower dimensions in the various longitudinal layers. Figures 19 to 22 show these radial distributions in both the ϕ and the u layers, for both electrons and π's. The rejection power contained in the longitudinal and radial development is given in Table 3 for a 4 GeV/c sample. Applying an energy cut on the ϕ and (u + v) shelves only, provides a π/e rejection of $\sim$ 1/115; a shower radius cut on (u + v) yields another factor of $\sim$ 3, and with a radial cut in ϕ a final rejection of 1 in 410 is obtained. Compared to this simple application of "threshold" cuts, the correct maximum likelihood treatment improves these rejection figures only marginally. Table 3 summarizes these various rejection performances.

5.2 Operation at the ISR

In this section we describe the use of the energy information which is available from the detectors to form various trigger conditions.

The technique used to obtain the localized energy sums is shown in Fig. 10a. All discriminator outputs belonging to one coordinate of the calorimeter are OR-ed together. Since the signal so obtained does not have a time definition that is adequate for strobing signals coming from the faster detectors of our apparatus, this OR is gated by a fast signal coming from scintillator hodoscopes. A localized energy trigger is defined as a coincidence between the three gated OR's coming from the ϕ, u, and v sections of any calorimeter. This signal, which is available in $\sim$ 300 nsec, is used to start the digitization of all the ADC channels in the system. The analog signals to the ADCs are delayed in order to arrive with this signal in time. This requirement reduces the trigger rate to the kHz level, which is low enough to permit second-level trigger decisions before recording the event. These decisions are available within a few micro-seconds; if they are not satisfied, the digitization can be aborted and the electronics can be readied for data-taking in about 2 μsec.

One of the more refined decisions correlates the azimuthal position of a charged particle with the shower in the calorimeter. This "correlation" trigger was designed to accept electrons in the presence of a large π^0 background. In order to match the position resolution of the proportional wire chamber (80 wires) just in front of the calorimeter, with the 32 strips in the ϕ section of the calorimeter, an interpolation method for finding the shower centre is used. The interpolation is done with a delay line into which the signal from all ϕ strips is injected. At the output of the delay line a suitable circuit[13] converts the discrete position coordinate into continuous time information. The logical signals from the 80 wires of the proportional chamber are loaded into a shift register.

The outputs from the shift register and from the linear interpolation circuit go to a single coincidence circuit, the output of which is the correlation signal. The frequency of the shift register clock is adjusted to fit the relative spacing of the two detectors (Fig. 10b).

The event acceptance conditions we have used most frequently are:

i) "two-arm" energy deposit: a local deposition of energy above a threshold in the ϕ and (u + v) shelves in at least two calorimeters;

ii) correlation-correlation: a local deposition of energy above threshold in the ϕ and (u + v) shelves accompanied by a charged particle in the upstream detector. Two showers are required, either in the same or in different Q modules.

In Fig. 23 we show the efficiency of such a trigger requirement for a nominal threshold of 1 GeV for one calorimeter only. The shape of the efficiency curve, as a function of particle energy, is determined mainly by fluctuations in the shower development in the first six radiation lengths. The energy spectrum of particles incident on the calorimeters is also shown in Fig. 23, which, for our experimental geometry near 90° in the c.m. system, reflects the well-known steep fall as a function of the transverse momentum.

Folding of the incident spectrum with the trigger efficiency results in the spectrum of collected events; it shows that more than 50% of the collected events have an energy below the nominal threshold*). As an example of the kind of performance obtained, we show in Fig. 24 the invariant mass spectrum of dilepton events produced in pp collisions at the ISR.

The width of the J/ψ peak is consistent with the quoted energy resolution of the calorimeters; the clustering of 21 events around m_{ee} = 9.5 GeV represents the first observation of the T(9.5) at the ISR[4].

We conclude with some comments on the long-term operational performance of the detector system. A summary of faults that occurred during the operation at the ISR is given in Table 4. Usually at the beginning of operation a few of the 448 channels showed short circuits, caused by tiny metal slivers left over in the cryogenic plumbing. These failures could usually be "burned out" with a capacitor discharge. Some of the HV bypass capacitors short-circuited after a number of

---

*) To sharpen the energy threshold we have used a condition on the total energy in the module in addition to the localized energy threshold as a second-level trigger decision.

thermal cycles. In such a case the channel was operated with an external resistive divider at reduced high tension. The failures of these capacitors were erratic, are not understood, and cannot be prompted by short-term testing methods (thermal or electrical cycling). We had some failures of the internal electrical connections between the wires and the crimped-on connectors that mated with the feedthroughs. These failures were traced to dimensional changes in both the wires and the sleeves. Repair required the opening of the calorimeter, and the failures were eliminated by soldering of these connections.

Acknowledgements

We would like to thank the Experimental Support Group and the Engineering Group of the CERN ISR Division for their generous support. We are also grateful for the efficient help of J.C. Berset and co-workers with the electronics aspects of the detectors, to the staff of the CERN Central Workshops for the manufacture of the tanks, and for the efforts of K. Ratz and G. Dubois-Dauphin. We benefited from numerous discussions with Dr. V. Radeka.

REFERENCES

1) W.J. Willis and V. Radeka, Nuclear Instrum. Methods 120, 221 (1974).

2) C. Fabjan et al., Nuclear Instrum. Methods 141, 61 (1977).

3) C. Kourkoumelis, CERN 77-06 (1977).

4) J. Cobb et al., Phys. Letters 68B, 101 (1977); 72B, 273 (1977).

5) J. Cobb et al., Nuclear Instrum. Methods 140, 413 (1977).

6) J. Fischer et al., Nuclear Instrum. Methods 136, 19 (1976).

7) M. Harris, H. Meyer and G. Trinquart, R806 calorimeter design, construction, and testing, CERN-ISR Internal Note (Jan. 1977).

I. Wilson, Results of a stress analysis of a liquid argon vessel, ISR Technical Note (Jan. 1976).

8) E. Gatti et al., Considerations for the design of a time projection liquid argon ionization chamber, BNL 23988 (1977).

9) D. Hitlin et al., Nuclear Instrum. Methods 137, 225 (1976).

10) P. Rehak, private communication.

11) S.E. Derenzo et al., Phys. Rev. A 9, 2582 (1974).

12) CERN-Copenhagen-Lund-Rutherford-ISR Collaboration, private communication.

13) J. Lindsay, CERN-EP Division, private communication.

Table 1

Properties of calorimeter sections

Strip type	ϕ	u	v	θ
Shelf number	1	2	2	3, 4, 5
Ground plate	1.5 mm Pb for all			
Signal plate	(sandwich of 0.5 mm Cu, 1.0 mm glass fibre, 0.5 mm Cu)			1.5 mm Pb
No. of strips	32	64	64	16
No. of channels	32	32	32	16
Gap width (mm)	2.05	2.05	2.05	2.3
No. of gaps	14	6	8	44
No. of rad. lengths	2.6	1.1	1.4	11.9
$(dE/dx)\Delta x$ (MeV)	40	17	23	161
% of sampled energy in LA [a)]	18.6	18.6	18.6	18.4
Capacitance/strip (nF)	3.3	1.8	2.3	22
Noise (10^3 e)	14.6	10.4	12.2	39
Noise (MeV)	4.3	3.1	3.6	11.6
Coll. charge/GeV (pC)	0.388	0.386	0.386	0.381
Cal. capacitor (pF)	2.5	2.5	2.5	7.5
Blocking capacitor (nF)	25	25	25	100
Transformer ratio	9:48	9:48	9:48	3(3 in parallel):48
Detector preampl. cable length (m)	1	1	1	1
Cable impedance (Ω)	100	100	100	4

a) Including correction for dead space in the calorimeter (see Table 2).

Table 2

Insensitive region in Q-calorimeter

Object	Material	Thickness (mm)	Δ rad. length	(dE/dx)Δx (MeV)
Foam isolation	Plastic	50	0.023	1.97
Front wall	Al	20	0.222	8.74
First cell (before ϕ strips)	Pb LA Fe	1.5 Pb + 1 LA + 3 Fe	0.444	1.92 0.2 3.48
Plate at the end of 1st floor	Al	8	0.088	3.5
Plate at the end of 2nd floor	Al	8	0.088	3.5
Plate at the end of 3rd floor	Al	10	0.111	4.37
Plate at the end of 4th floor	Al	10	0.111	4.37

Table 3

Summary of the h/e rejection (including shower profile information)

Cut	η_e (%)	η_π (%)	η_π/η_e
$Q_\phi > Q_\phi^{cut}$; $Q_{u+v} > Q_{u+v}^{cut}$	85	0.75	1/115
as above + $(\sigma_u < \sigma_u^{cut}) \cdot (\sigma_v < \sigma_v^{cut})$	83.6	0.27	1/310
as above + $\sigma_\phi < \sigma_\phi^{cut}$	82.8	0.20	1/410

Table 4

Summary of faults in the calorimeter system (period: Spring 1975-Spring 1978, total of ∿ 450 channels)

Type	Origin	Remedy	Frequency
Short circuit in a strip	Small metal slivers (Pb or others).	"Burn-out" with HV discharge (while cold); always successful.	Few strips usually after cool-down; during operation: ∿ 1/month.
Short circuit in a strip	Touching strips owing to improper thermal cycling.	Removal and disassembly of calorimeter.	Twice during operation.
Contaminated LA	Mostly due to improper flushing.	Replacement.	LA was replaced ∿ twice per year (long shutdowns, limited storage, etc.).
Loss of LA	Faulty operation of cryogenics system.	Replacement.	Twice during operation, before automatic relief valves were installed.
Short circuit in HV blocking capacitors	Unknown.	Temporarily, by supplying externally reduced potential; exchange.	At few % level for large (100 nF) capacitors; none after replacement with potted capacitors.
Defective preamps.	Weak components(?).	Exchange.	∿ once per month.

Figure captions

Fig. 1 : Schematic cross-section of the apparatus. In the modular detectors, electrons are identified through transition radiation and electromagnetic showers in the calorimeters.

Fig. 2 : Electrode arrangement for localization and measurement of transverse and longitudinal distribution of the showers.

Fig. 3 : Artist's view of calorimeter tank.

Fig. 4 : View of large feedthrough used for flat ribbon cables. The metal blades are dimensioned to mate with standard printed-circuit edge connectors.

Fig. 5 : Detail of tank support. Also shown are the small support arms for scintillators and transition radiation detectors.

Fig. 6 : Cross-section through calorimeter module showing the support of the individual "sandwiches".

Fig. 7 : Simplified diagram of the LA and LN_2 cryogenics system.

Fig. 8 : Long-term stability of the LA as monitored with the π^0 mass peak using the "nominal" charge-energy calibration. This record covers a period of about four months.

Fig. 9 : Block diagram of the linear electronics.

Fig. 10 : a) Summing of signals from adjacent strips to form the localized energy requirement.

b) "Correlation" logic used to correlate the position of electromagnetic showers in the calorimeter with signals from charged particles in the LPWCs.

Fig. 11 : Observed calorimeter response as a function of incident electron energy.

Fig. 12 : Observed pulse-height distributions for electrons of various incident momenta. The slight asymmetry in the low-energy side resulted from bremsstrahlung losses in the beam.

Fig. 13 : Position resolution of electromagnetic showers.

Fig. 14 : Iso-efficiency curves for 4 GeV/c electrons showing the pion acceptance for varying combinations of energy requirements in the ϕ and (u + v) shelves.

Fig. 15 : Correlation between charge produced in the ϕ shelf versus charge in the (u + v) shelf (4 GeV/c electrons).

Fig. 16 : Correlation between charge produced in the ϕ shelf versus charge in the (u + v) shelf (4 GeV/c pions).

Fig. 17 : Fluctuation in the longitudinal energy deposit Q(u) - Q(v) (arbitrary units) versus the total energy deposited, Q(u) + Q(v) (4 GeV/c electrons).

Fig. 18 : Fluctuation in the longitudinal energy deposit Q(u) - Q(v) (arbitrary units) versus the total energy deposited, Q(u) + Q(v) (4 GeV/c pions).

Fig. 19 : Radial shower dimension σ_ϕ in the ϕ shelf as a function of Q_ϕ (4 GeV/c electrons).

Fig. 20 : Radial shower dimension σ_ϕ in the ϕ shelf as a function of Q_ϕ (4 GeV/c pions).

Fig. 21 : Radial shower dimension of 4 GeV/c electrons in the u shelf.

Fig. 22 : Radial shower dimension of 4 GeV/c pions in the u shelf.

Fig. 23 : Trigger efficiency of energy cuts in the ϕ and (u + v) shelves set at a nominal threshold of 1 GeV total electromagnetic energy.

Fig. 24 : Invariant mass spectrum of dileptons produced in pp collisions at the ISR. The dielectron continuum is bracketed by the J/ψ and the T. The solid line gives the estimated background.

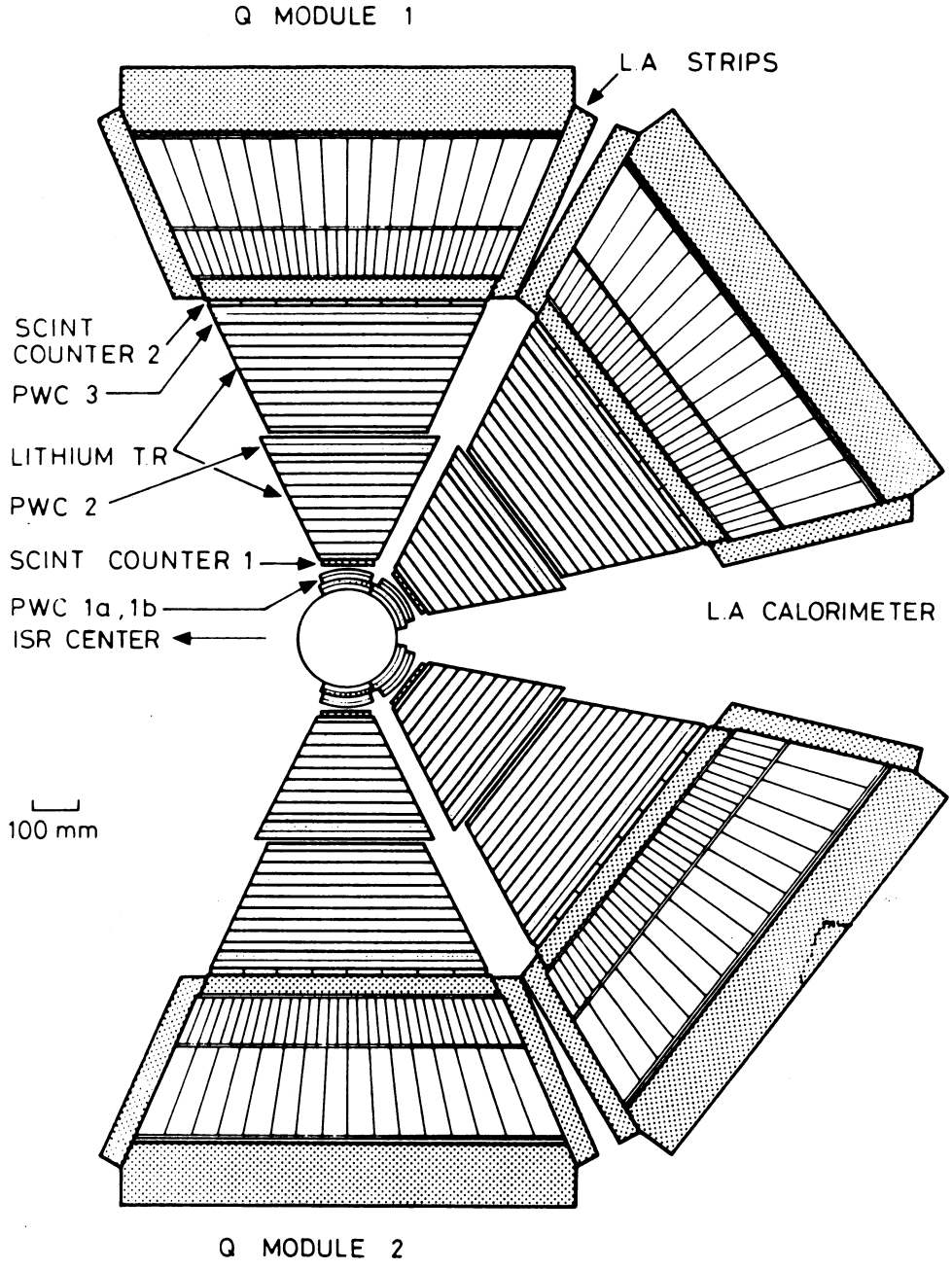
Q MODULE 1
L.A STRIPS
SCINT
COUNTER 2
PWC 3
LITHIUM T.R
PWC 2
SCINT COUNTER 1
PWC 1a, 1b
ISR CENTER
L.A CALORIMETER
100 mm
Q MODULE 2

Fig. 1

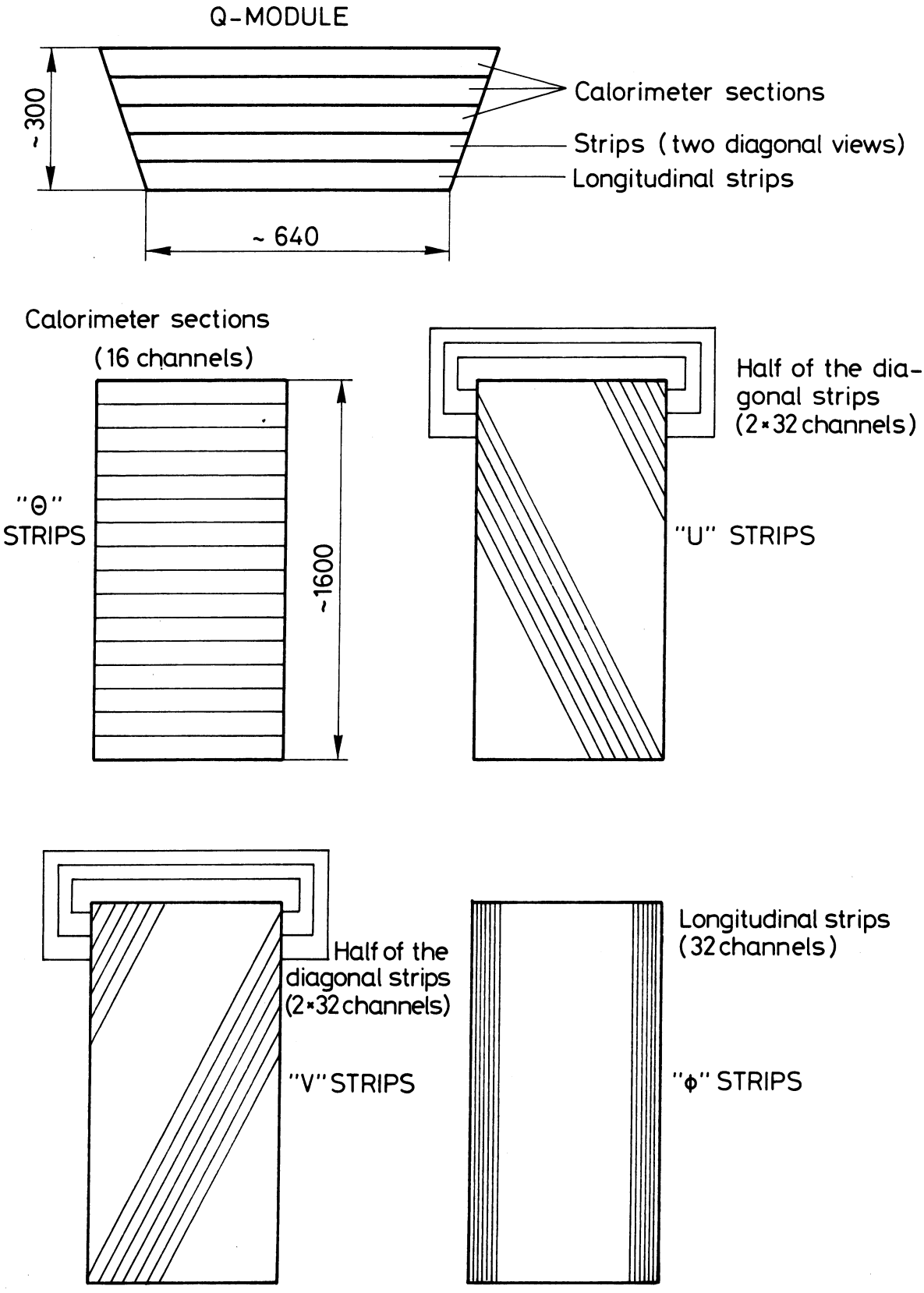
Q-MODULE
~ 300
~ 640
Calorimeter sections
Strips (two diagonal views)
Longitudinal strips
Calorimeter sections
(16 channels)
"Θ"
STRIPS
~1600
Half of the dia-
gonal strips
(2×32 channels)
"U" STRIPS
Half of the
diagonal strips
(2×32 channels)
"V" STRIPS
Longitudinal strips
(32 channels)
"φ" STRIPS

Fig. 2

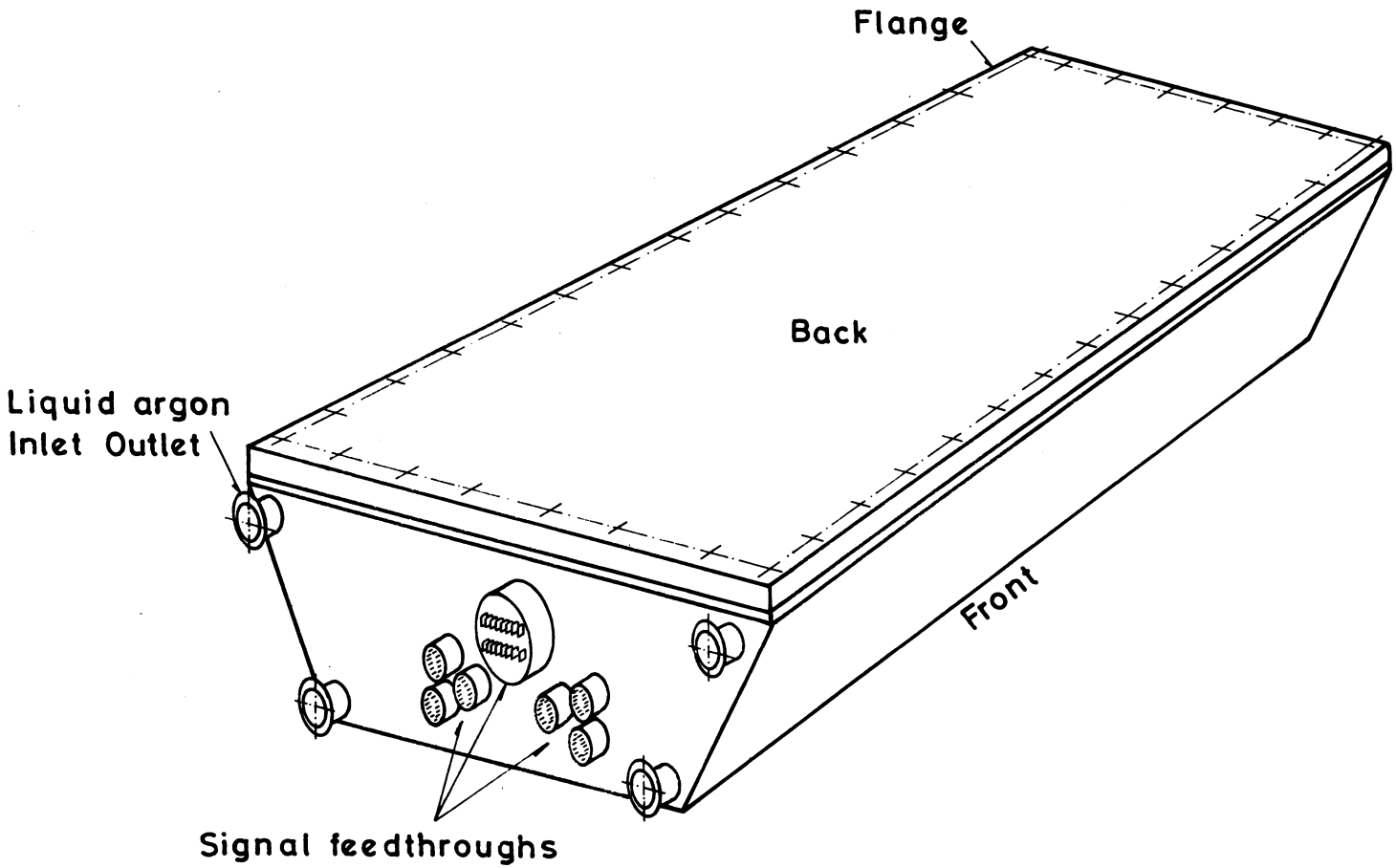
Flange
Back
Liquid argon
Inlet Outlet
Front
Signal feedthroughs

Fig. 3

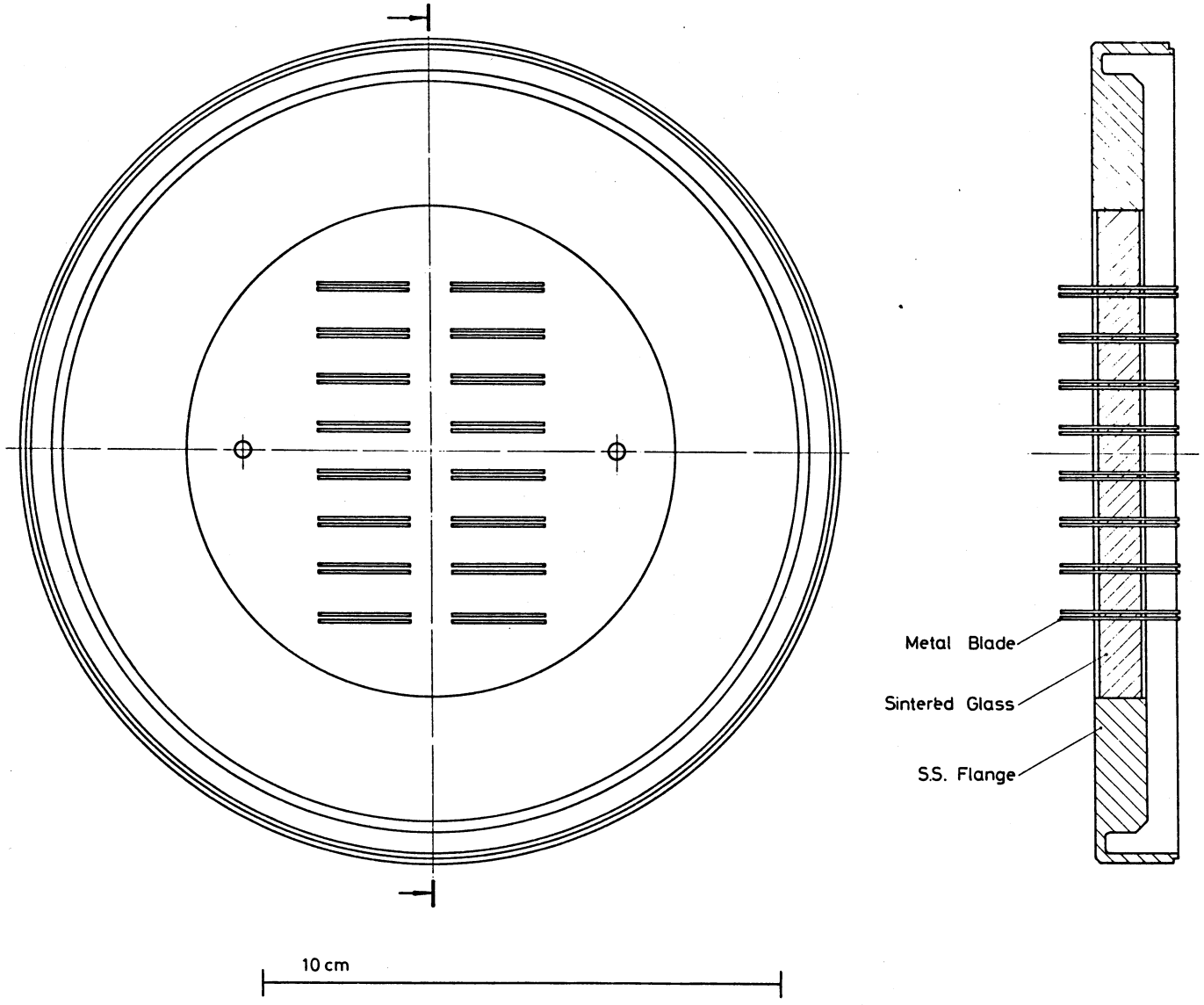

Fig. 4

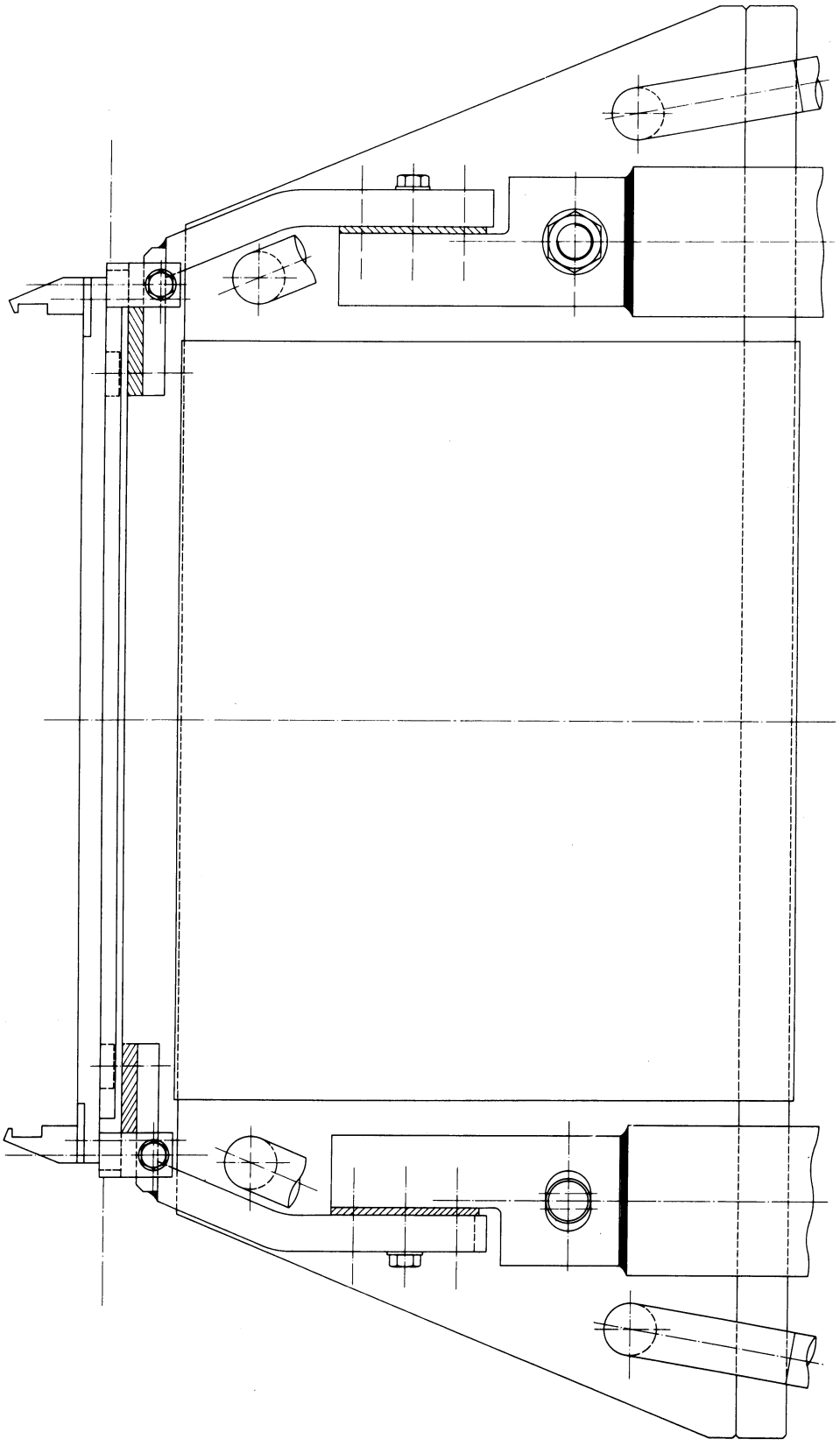

Fig. 5

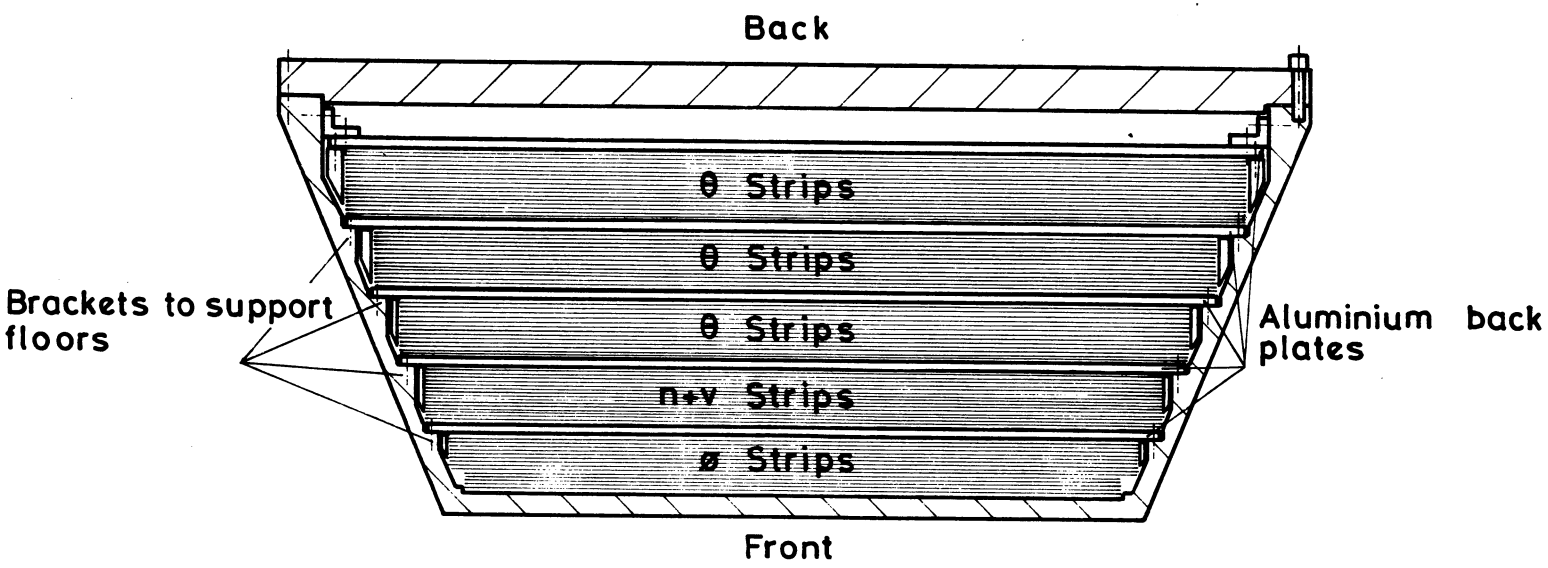
Back
θ Strips
θ Strips
θ Strips
n+v Strips
ø Strips
Front
Brackets to support floors
Aluminium back plates

Fig. 6

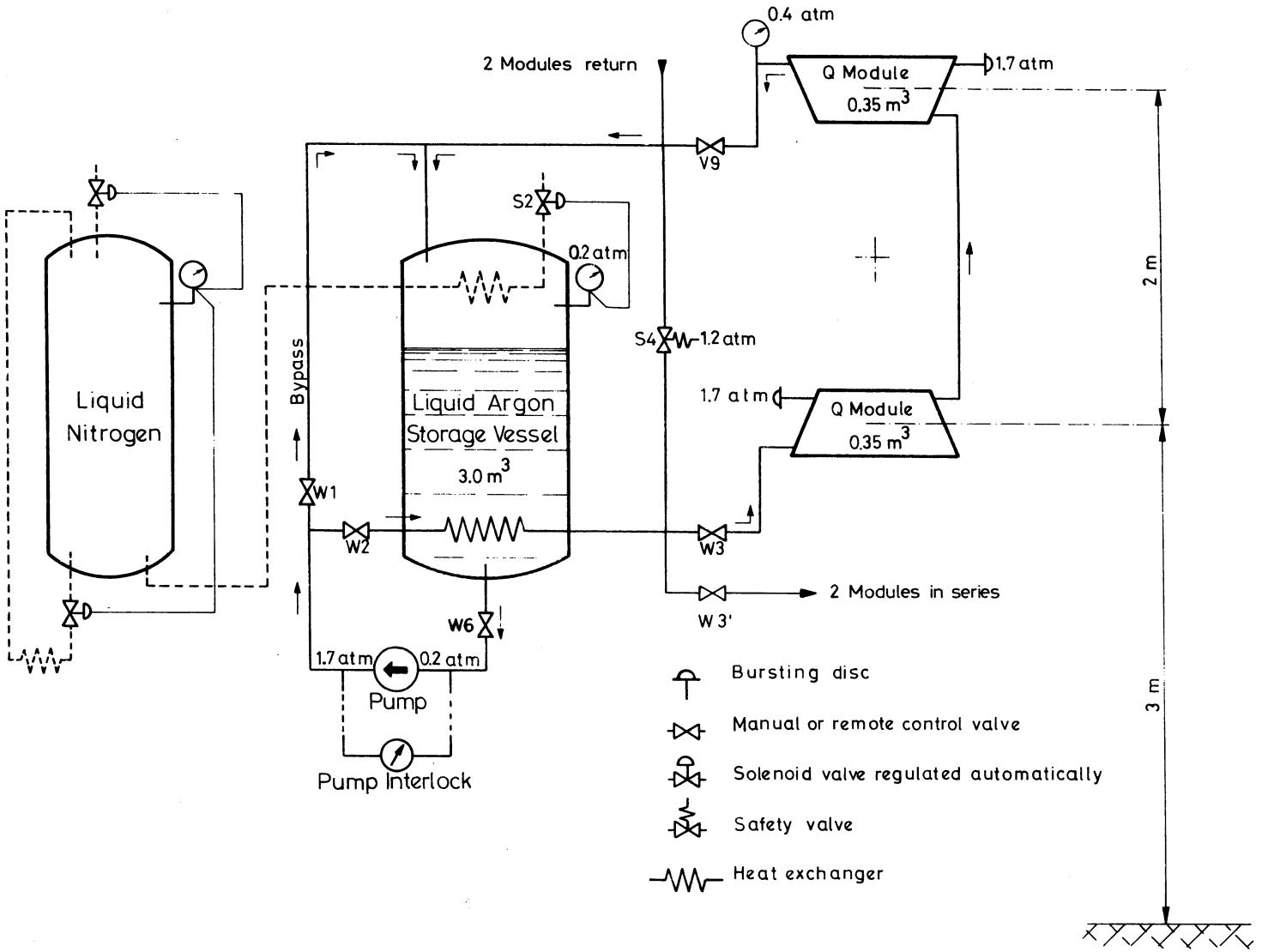
0.4 atm
2 Modules return
Q Module
0.35 m3
1.7 atm
V9
S2
0.2 atm
S4
1.2 atm
2 m
Liquid
Nitrogen
Bypass
Liquid Argon
Storage Vessel
3.0 m3
1.7 atm
Q Module
0.35 m3
W1
W2
W3
2 Modules in series
W 3'
W6
1.7 atm
0.2 atm
Pump
Pump Interlock
3 m
Bursting disc
Manual or remote control valve
Solenoid valve regulated automatically
Safety valve
Heat exchanger

Fig. 7

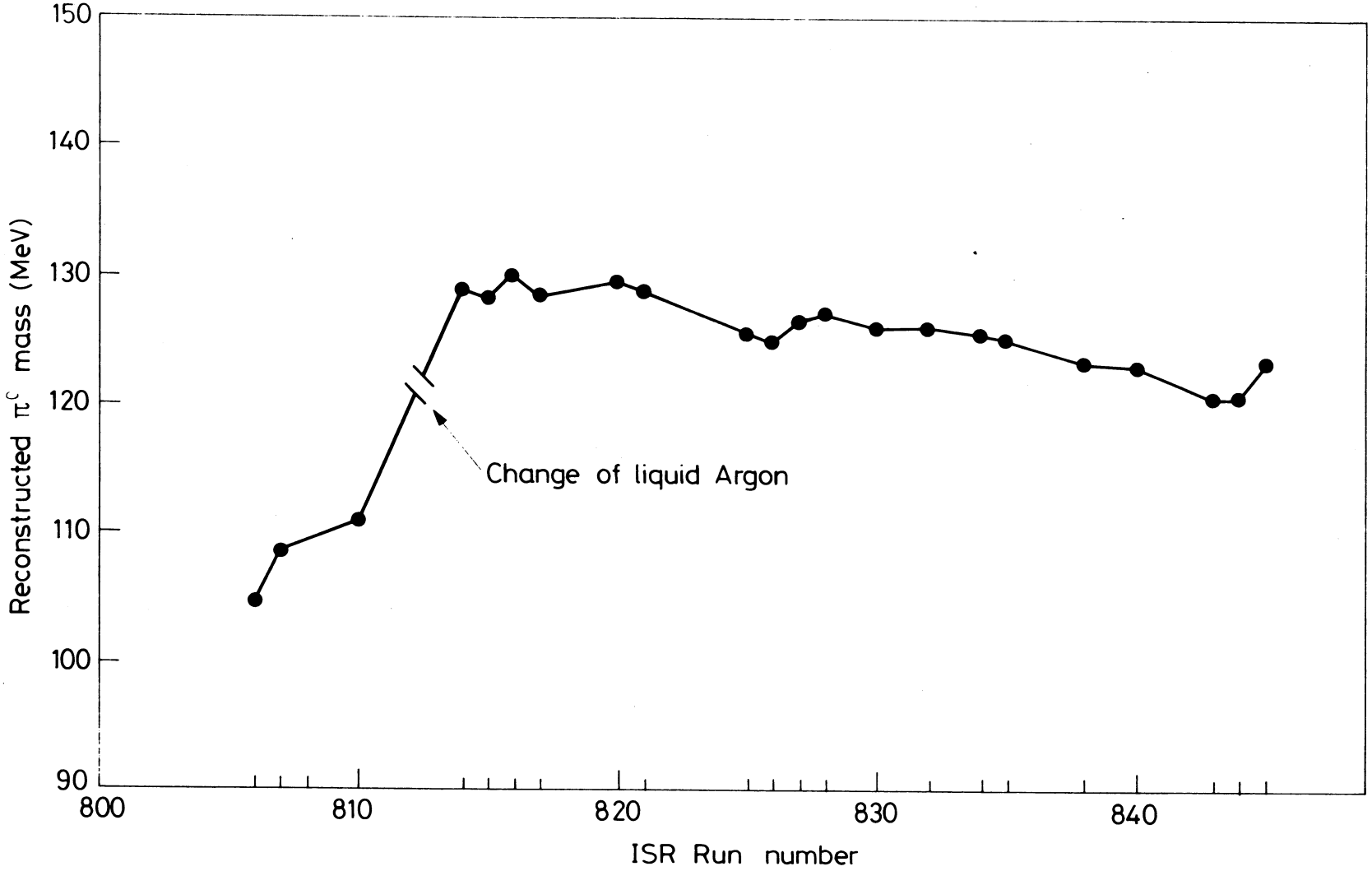
150
140
130
120
110
100
90
Reconstructed π^c mass (MeV)
Change of liquid Argon
800
810
820
830
840
ISR Run number

Fig. 8

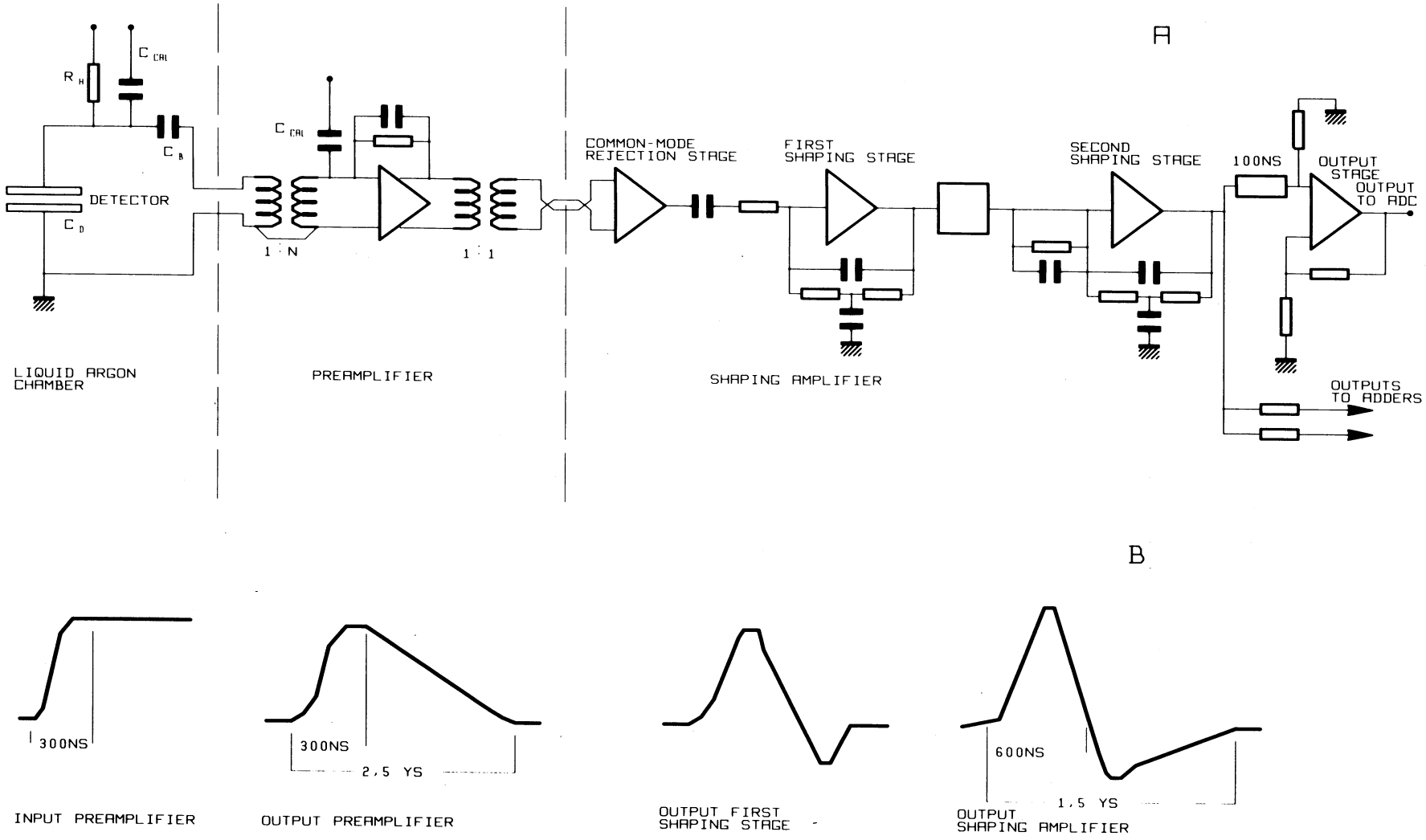
A
R_H
C_{CAL}
C_B
DETECTOR
C_D
C_{CAL}
1 : N
1 : 1
COMMON-MODE REJECTION STAGE
FIRST SHAPING STAGE
SECOND SHAPING STAGE
100NS
OUTPUT STAGE
OUTPUT TO ADC
OUTPUTS TO ADDERS
LIQUID ARGON CHAMBER
PREAMPLIFIER
SHAPING AMPLIFIER
B
300NS
INPUT PREAMPLIFIER
300NS
2,5 YS
OUTPUT PREAMPLIFIER
OUTPUT FIRST SHAPING STAGE
600NS
1,5 YS
OUTPUT SHAPING AMPLIFIER

Fig. 9

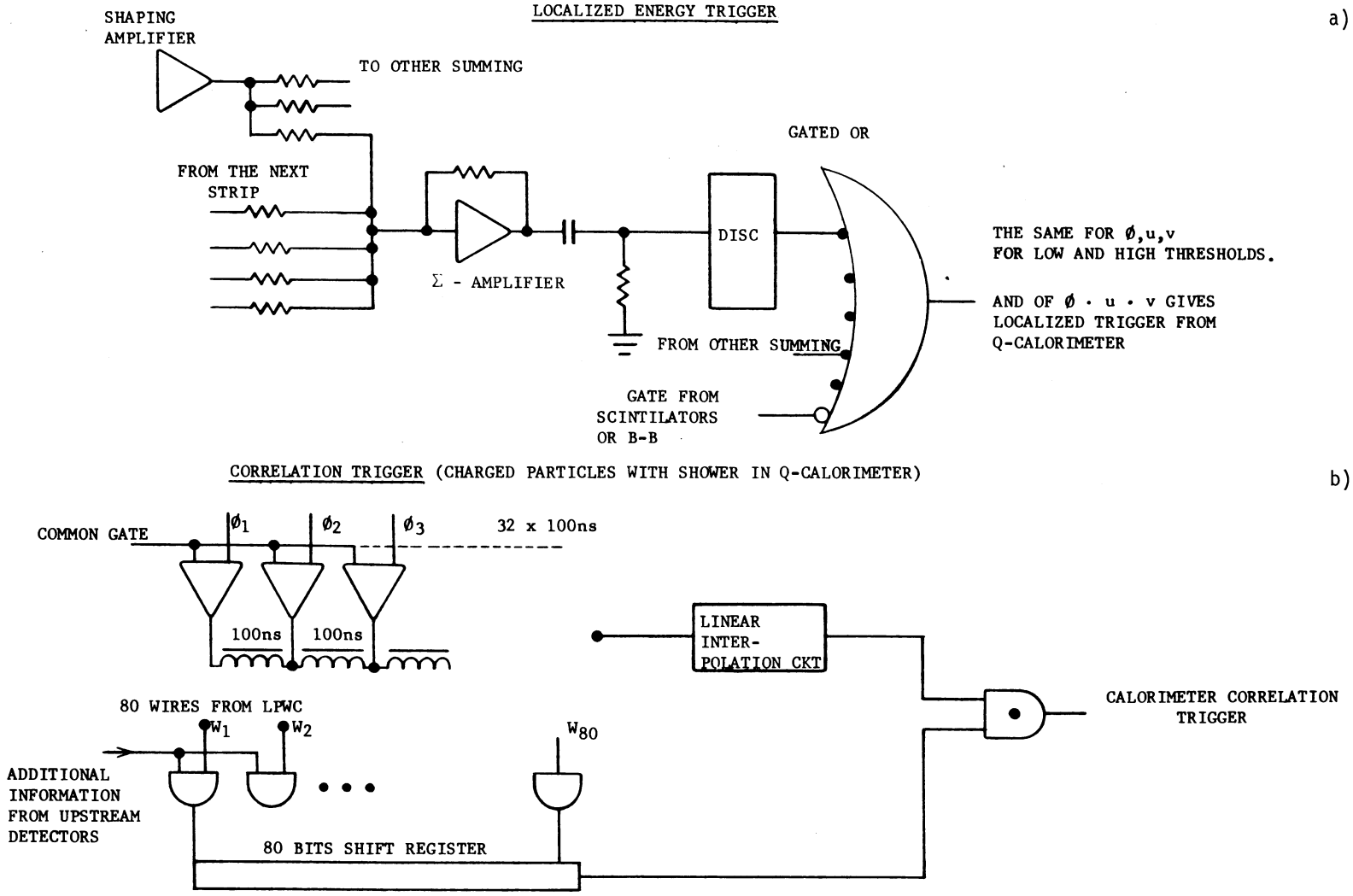
LOCALIZED ENERGY TRIGGER
a)
SHAPING AMPLIFIER
TO OTHER SUMMING
GATED OR
FROM THE NEXT STRIP
Σ - AMPLIFIER
DISC
THE SAME FOR Ø,u,v FOR LOW AND HIGH THRESHOLDS.
AND OF Ø · u · v GIVES LOCALIZED TRIGGER FROM Q-CALORIMETER
FROM OTHER SUMMING
GATE FROM SCINTILATORS OR B-B
CORRELATION TRIGGER (CHARGED PARTICLES WITH SHOWER IN Q-CALORIMETER)
b)
COMMON GATE
Ø1
Ø2
Ø3
32 x 100ns
100ns
100ns
LINEAR INTER-POLATION CKT
CALORIMETER CORRELATION TRIGGER
80 WIRES FROM LPWC
W1
W2
W80
ADDITIONAL INFORMATION FROM UPSTREAM DETECTORS
80 BITS SHIFT REGISTER

Fig. 10

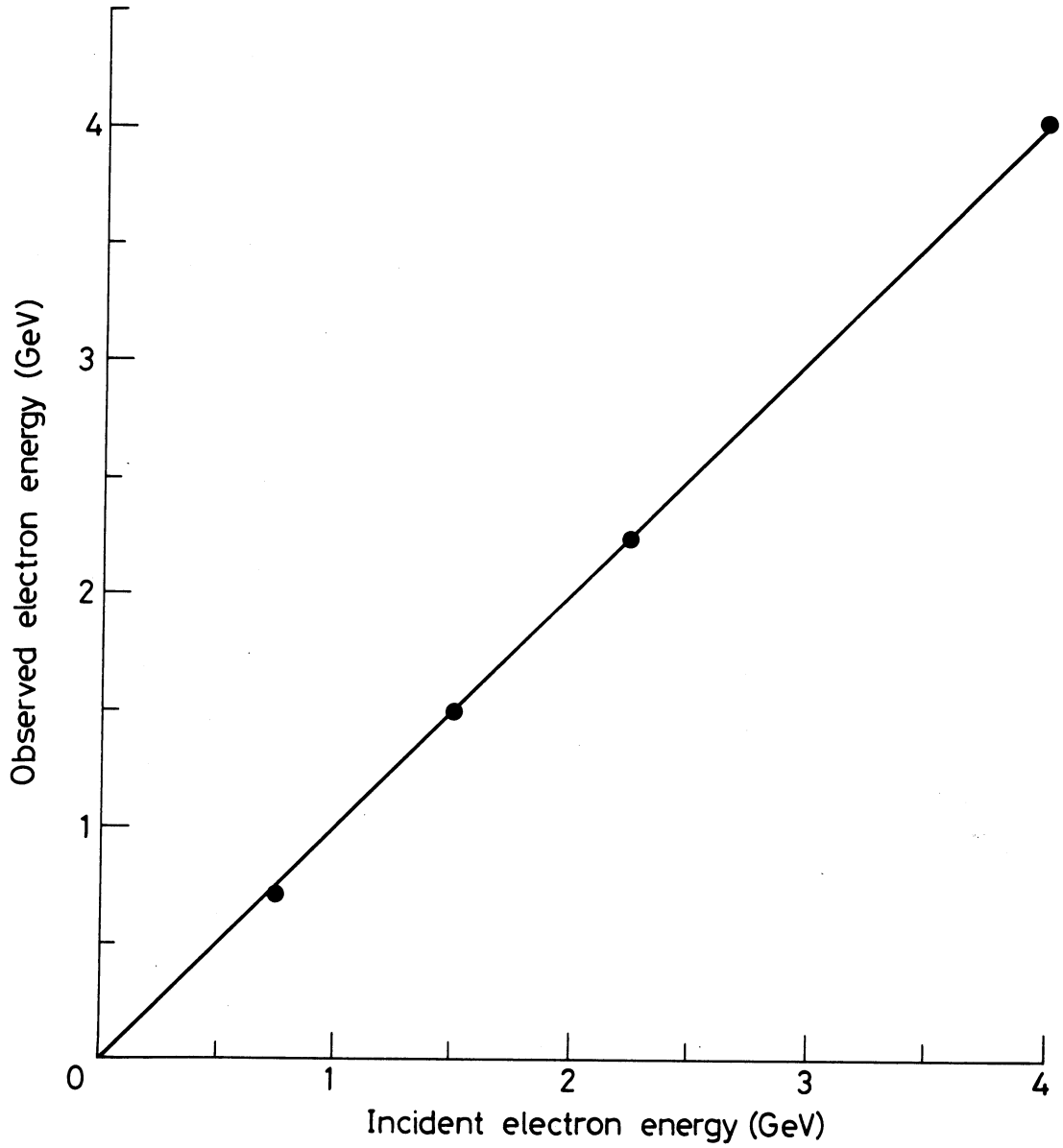
Observed electron energy (GeV)
Incident electron energy (GeV)
0
1
2
3
4
1
2
3
4

Fig. 11

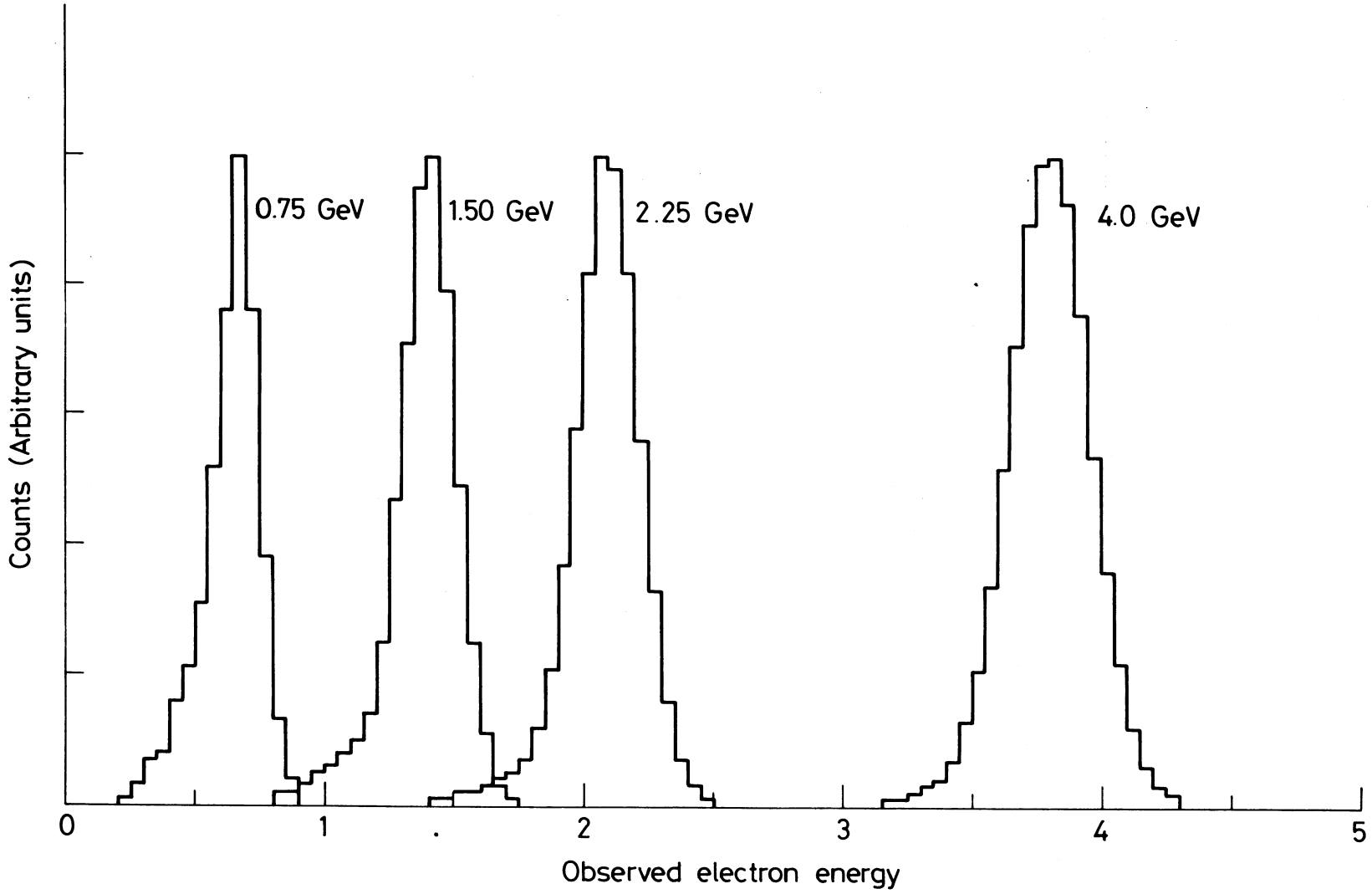
0.75 GeV
1.50 GeV
2.25 GeV
4.0 GeV
Counts (Arbitrary units)
0
1
2
3
4
5
Observed electron energy

Fig. 12

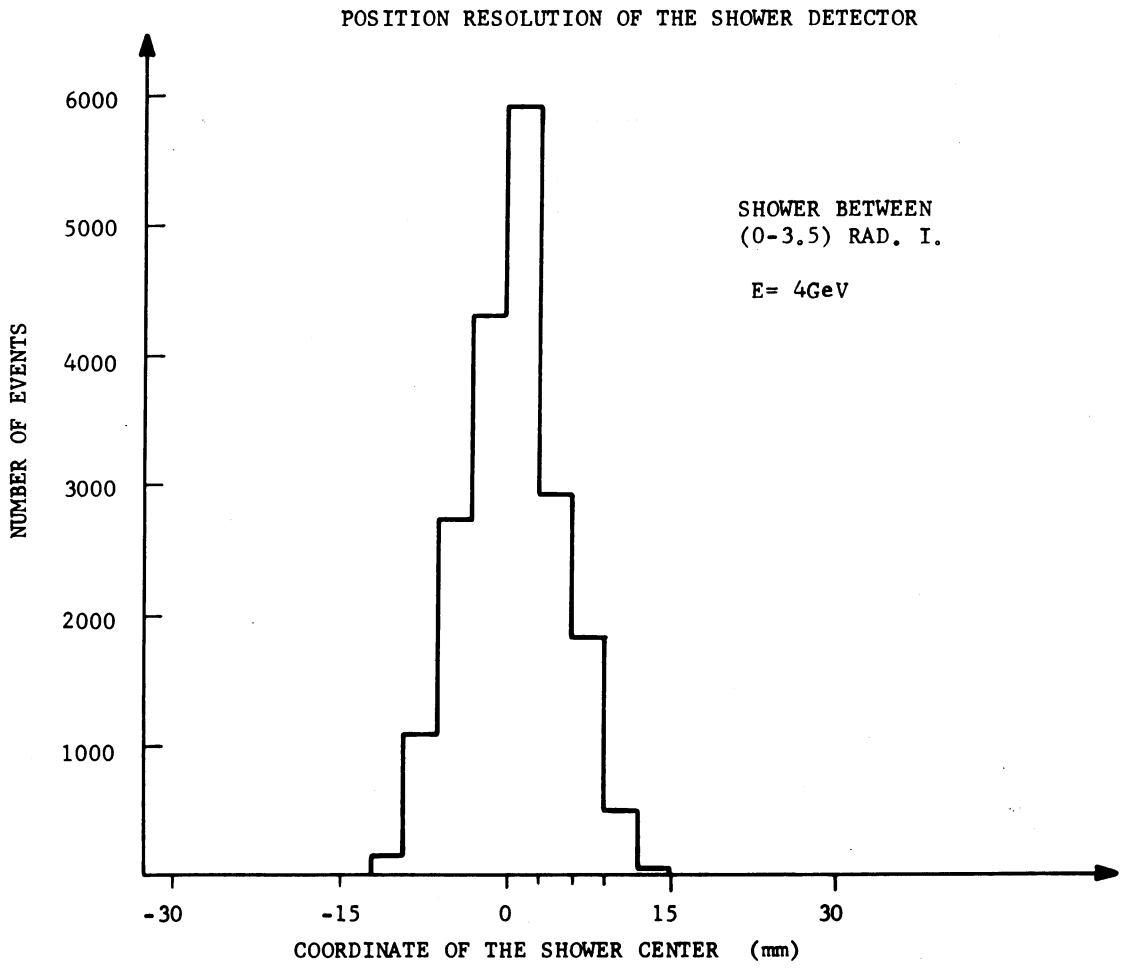
POSITION RESOLUTION OF THE SHOWER DETECTOR
NUMBER OF EVENTS
6000
5000
4000
3000
2000
1000
SHOWER BETWEEN
(0-3.5) RAD. I.
E= 4GeV
-30
-15
0
15
30
COORDINATE OF THE SHOWER CENTER (mm)

Fig. 13

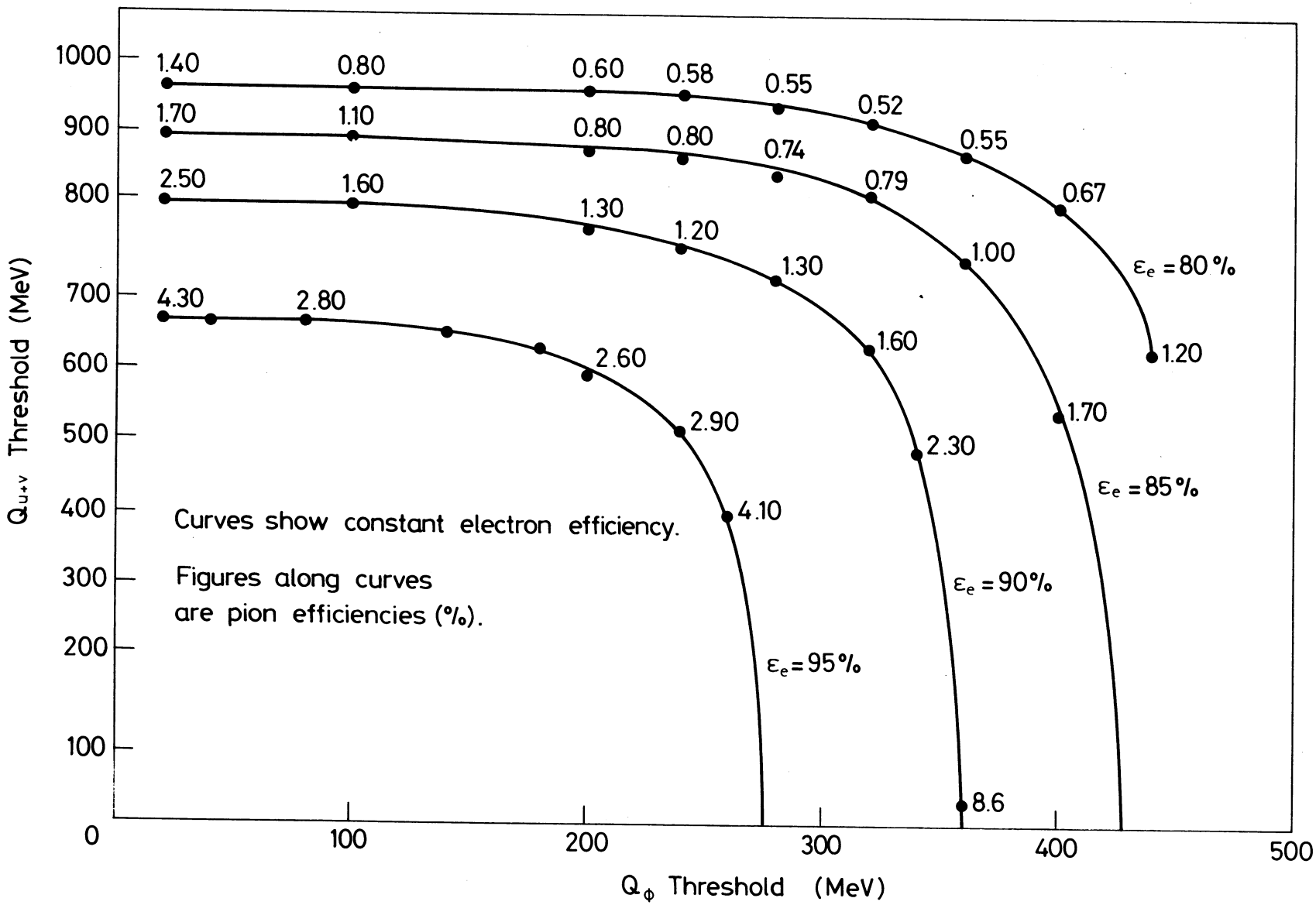
1000
900
800
700
600
500
400
300
200
100
0
100
200
300
400
500
Q_{u+v} Threshold (MeV)
Q_ϕ Threshold (MeV)
1.40
0.80
0.60
0.58
0.55
0.52
0.55
0.67
1.20
$\varepsilon_e = 80\%$
1.70
1.10
0.80
0.80
0.74
0.79
1.00
1.70
$\varepsilon_e = 85\%$
2.50
1.60
1.30
1.20
1.30
1.60
2.30
8.6
$\varepsilon_e = 90\%$
4.30
2.80
2.60
2.90
4.10
$\varepsilon_e = 95\%$
Curves show constant electron efficiency.
Figures along curves
are pion efficiencies (%).

Fig. 14

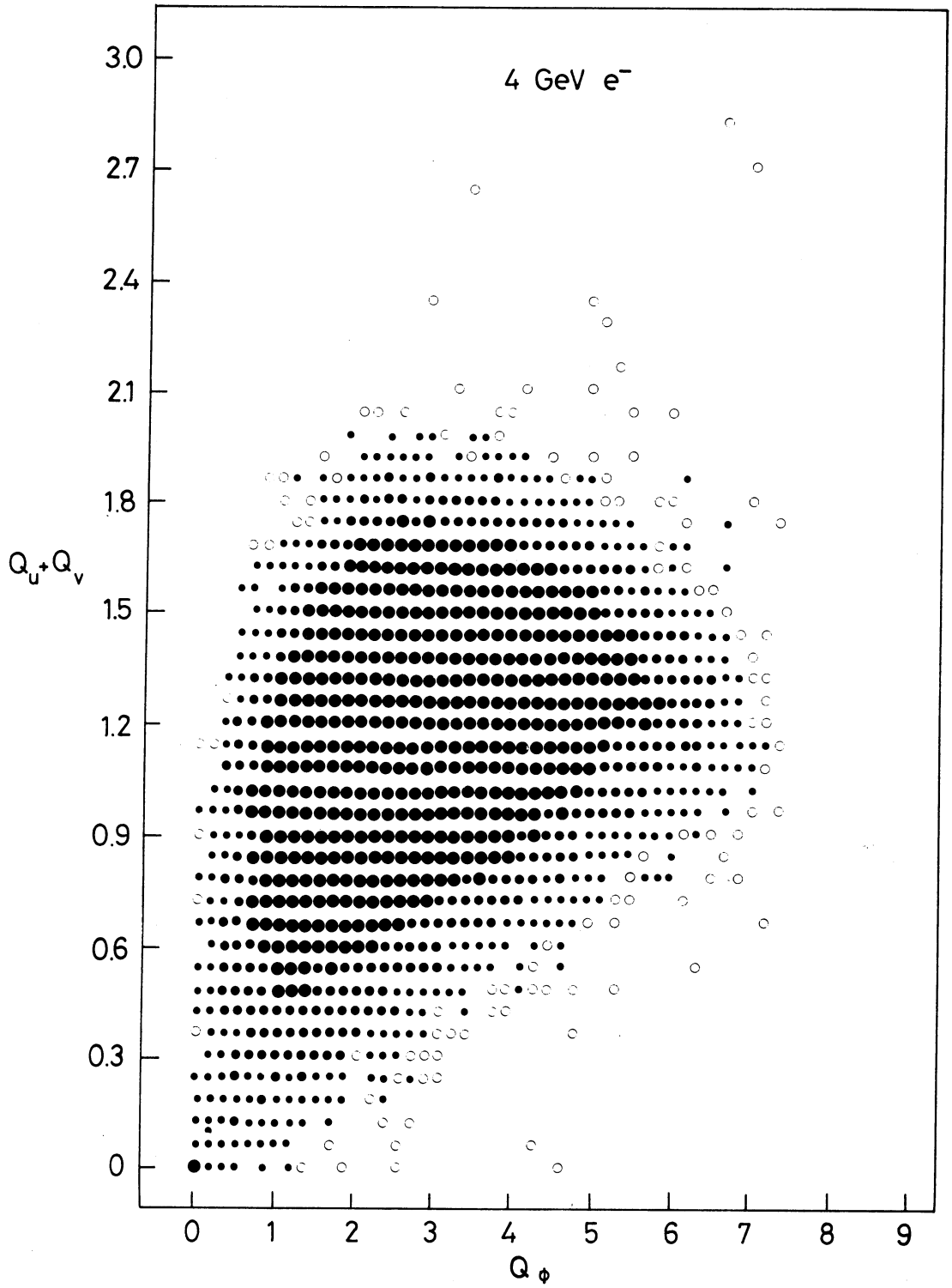

Fig. 15

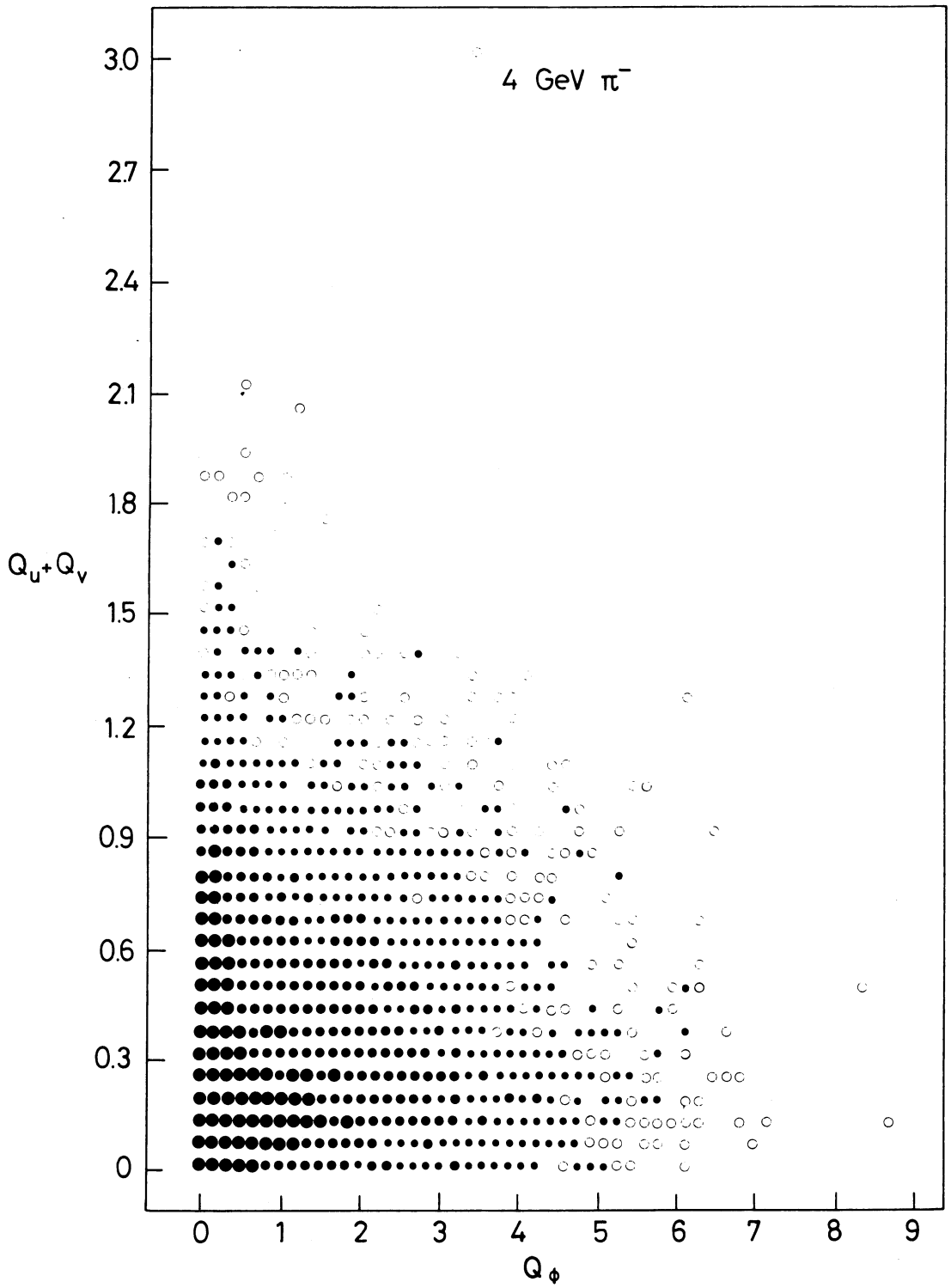

Fig. 16

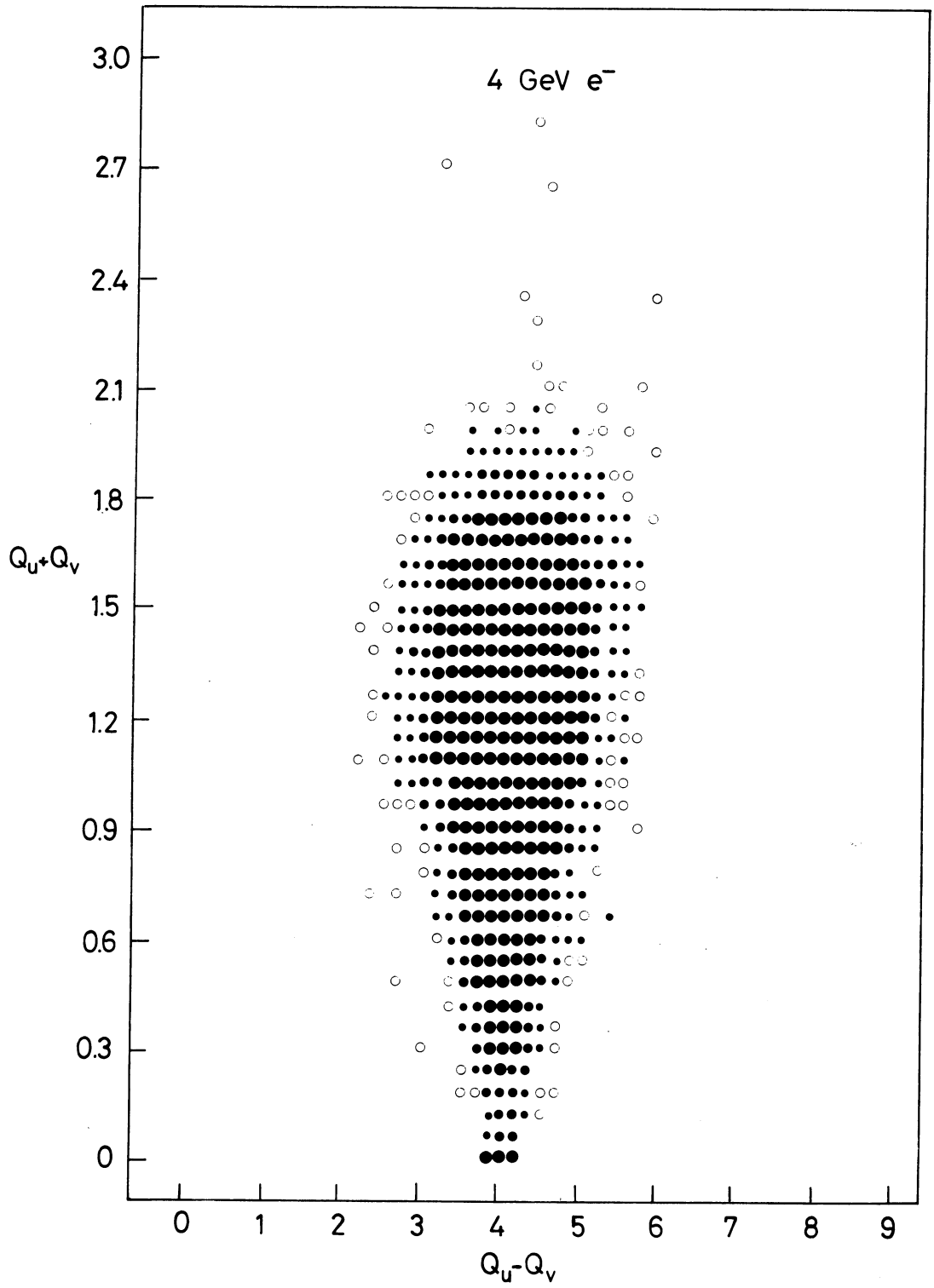

Fig. 17

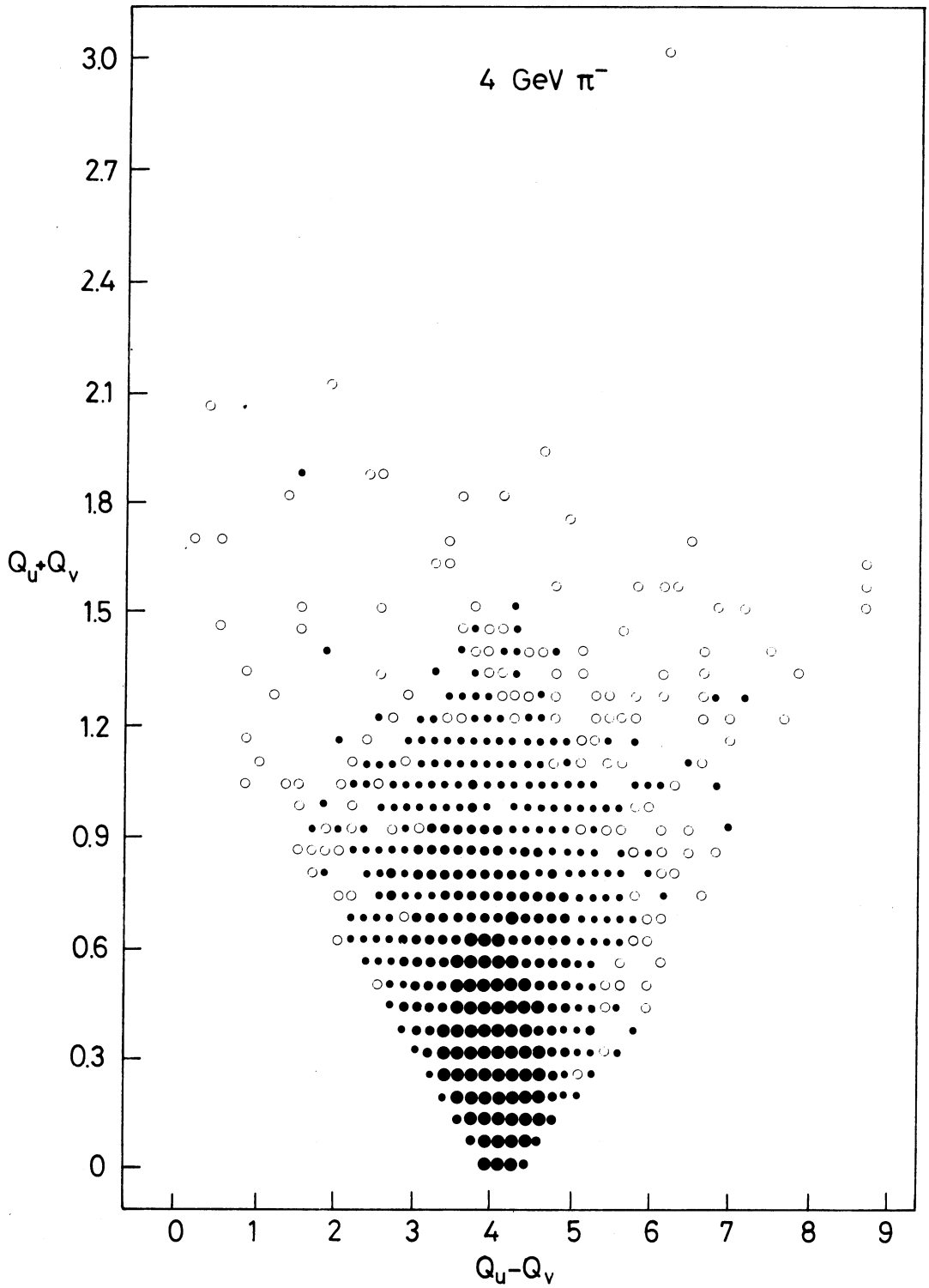

Fig. 18

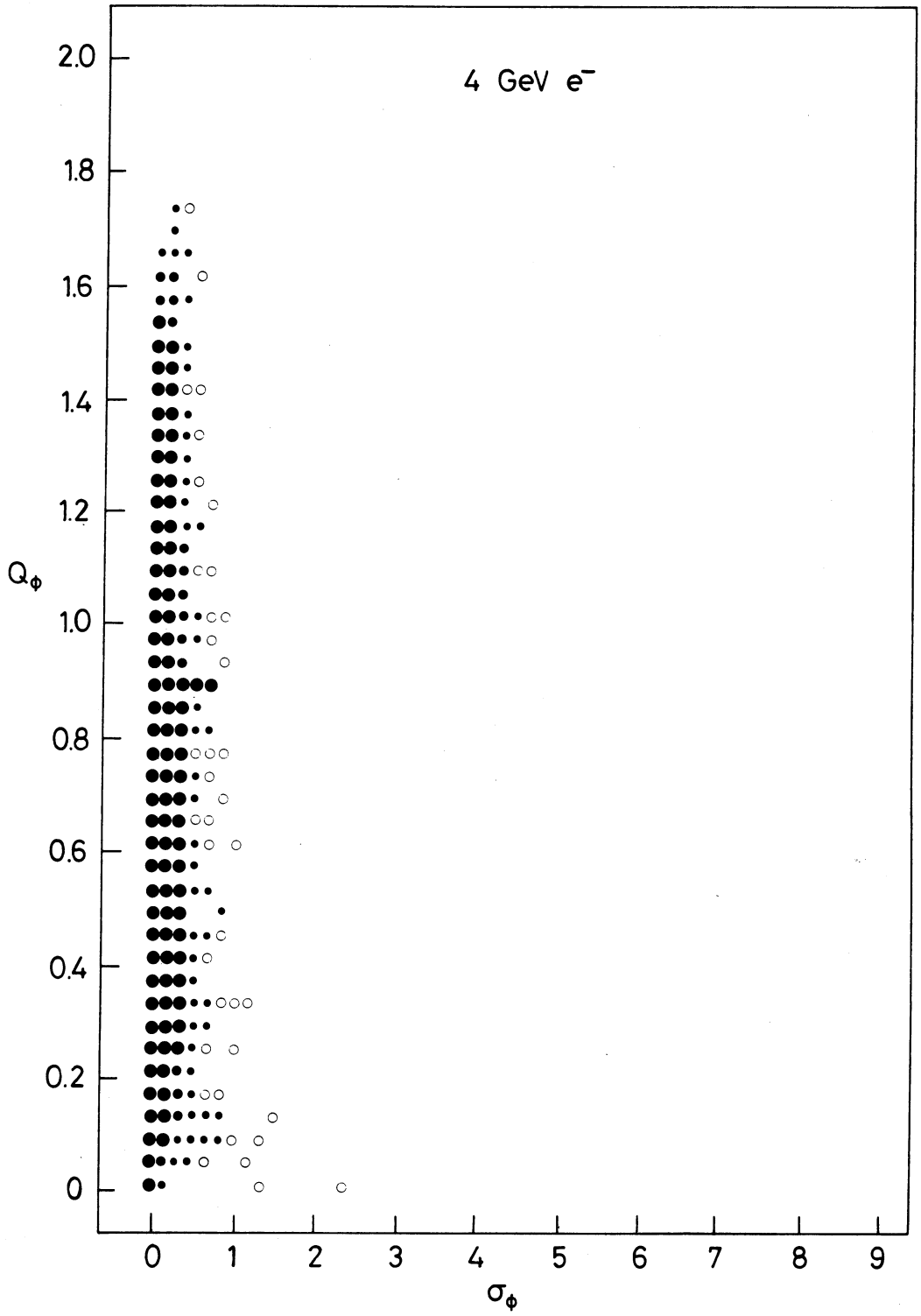

Fig. 19

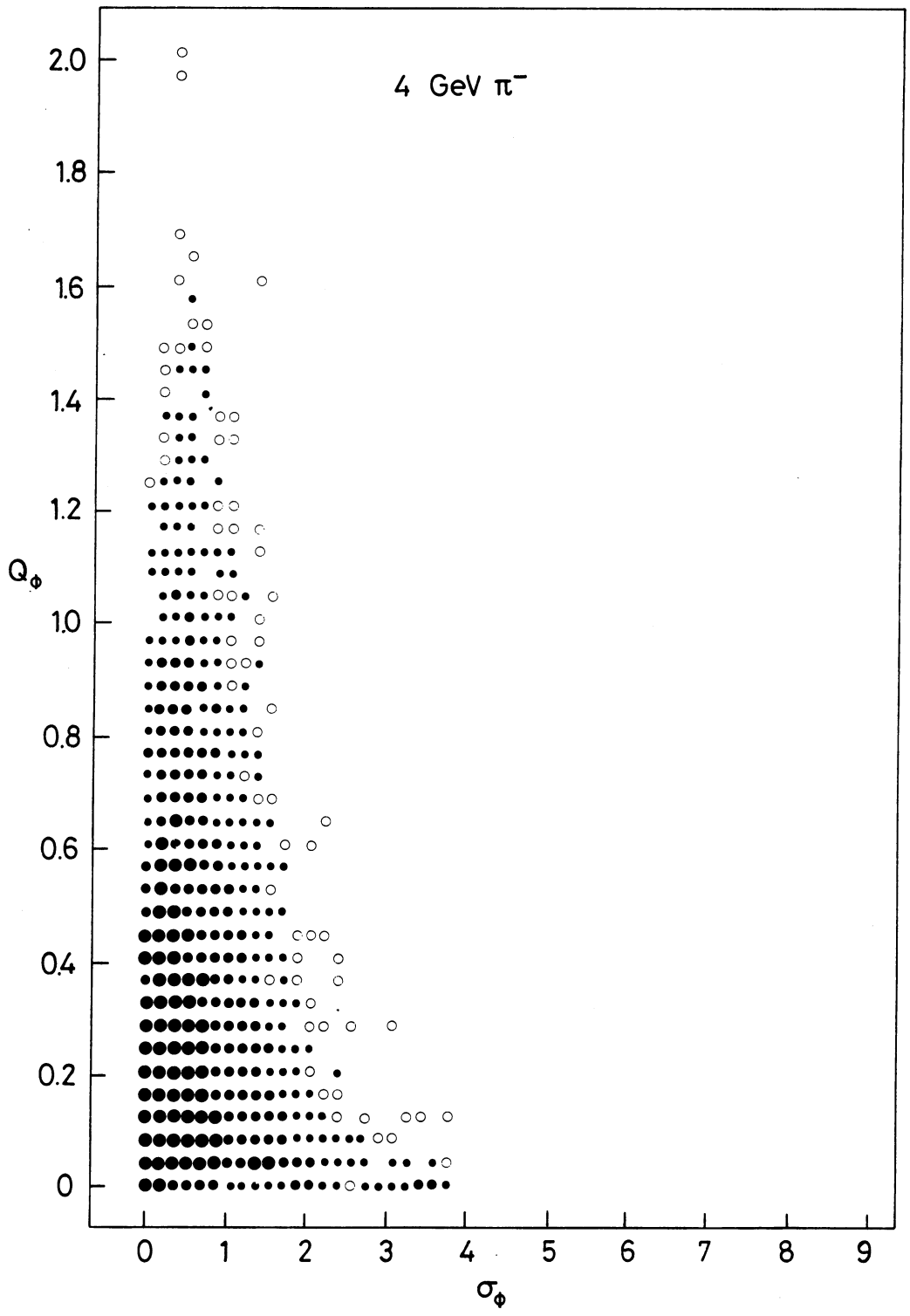

Fig. 20

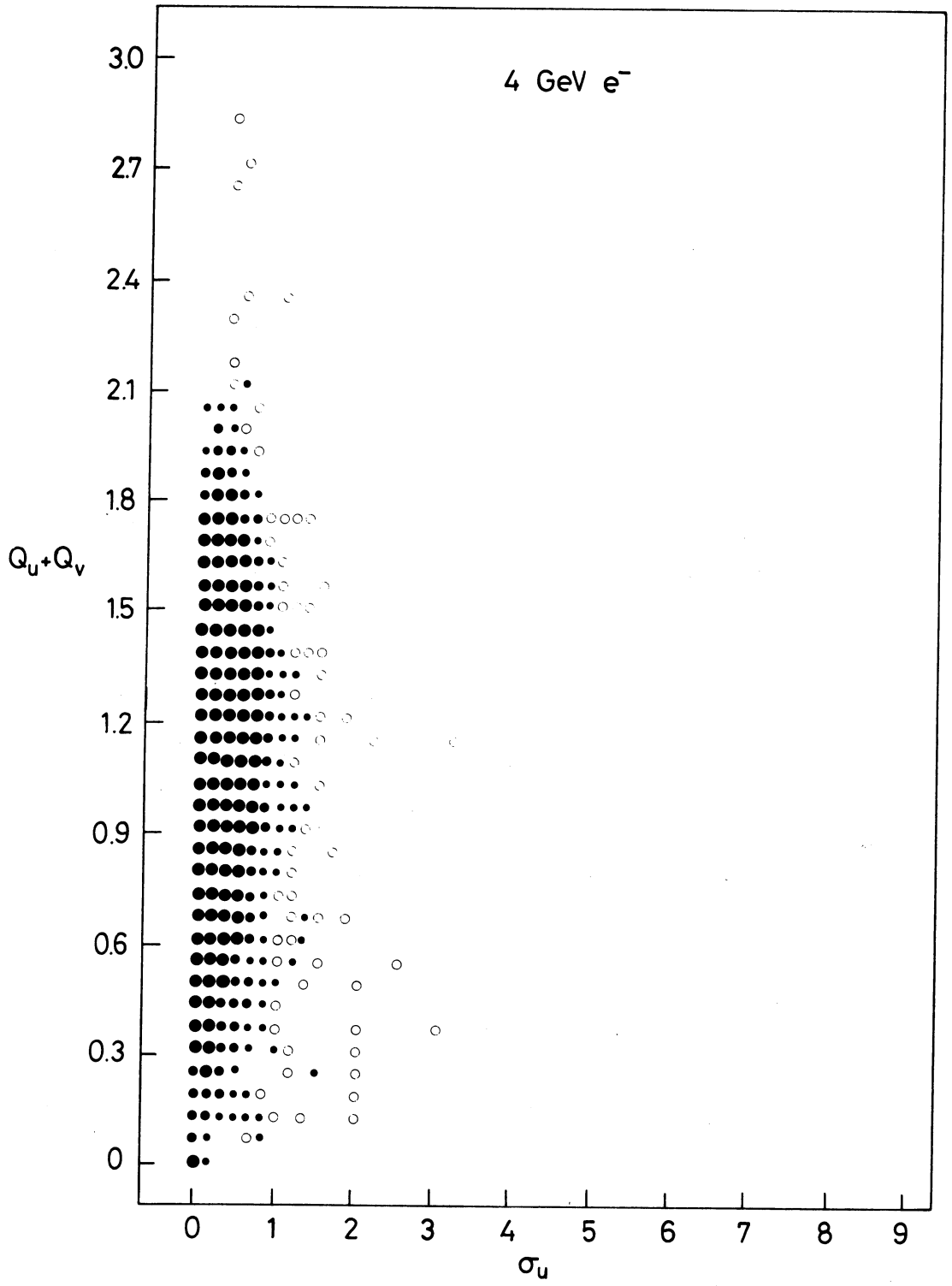

Fig. 21

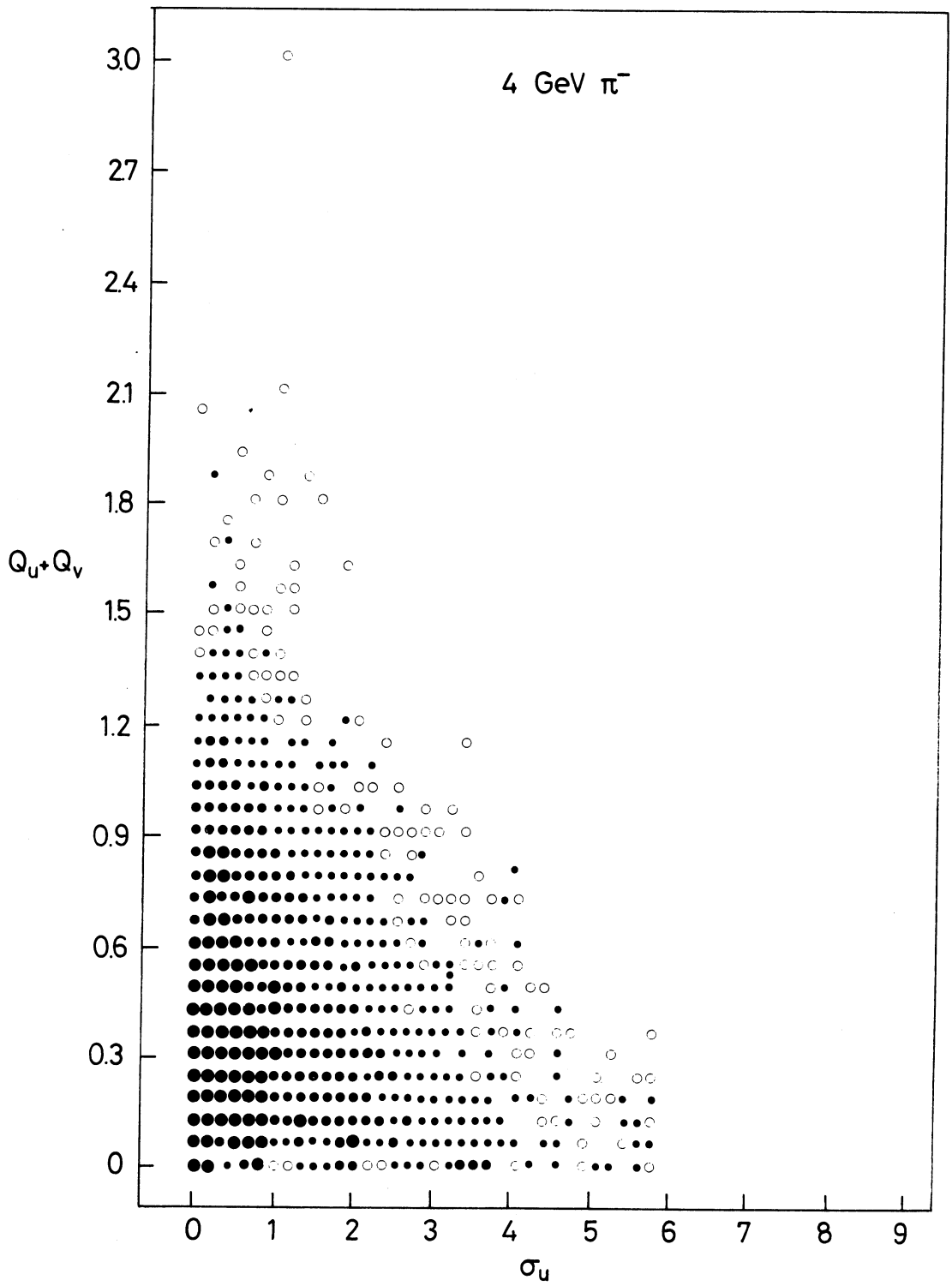

Fig. 22

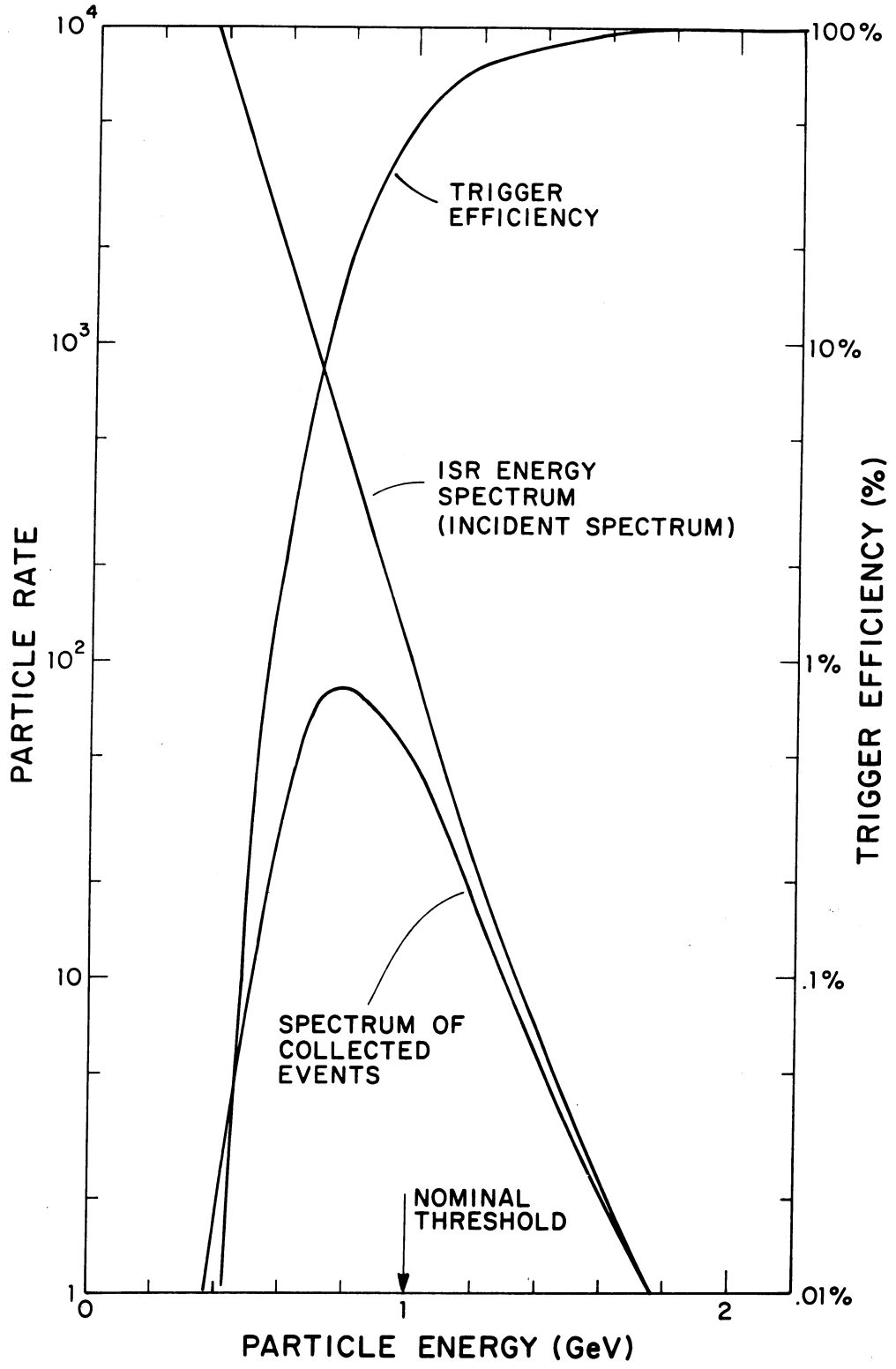
10^4
10^3
10^2
10
1
0
1
2
100%
10%
1%
.1%
.01%
PARTICLE RATE
TRIGGER EFFICIENCY (%)
PARTICLE ENERGY (GeV)
TRIGGER EFFICIENCY
ISR ENERGY SPECTRUM (INCIDENT SPECTRUM)
SPECTRUM OF COLLECTED EVENTS
NOMINAL THRESHOLD

Fig. 23

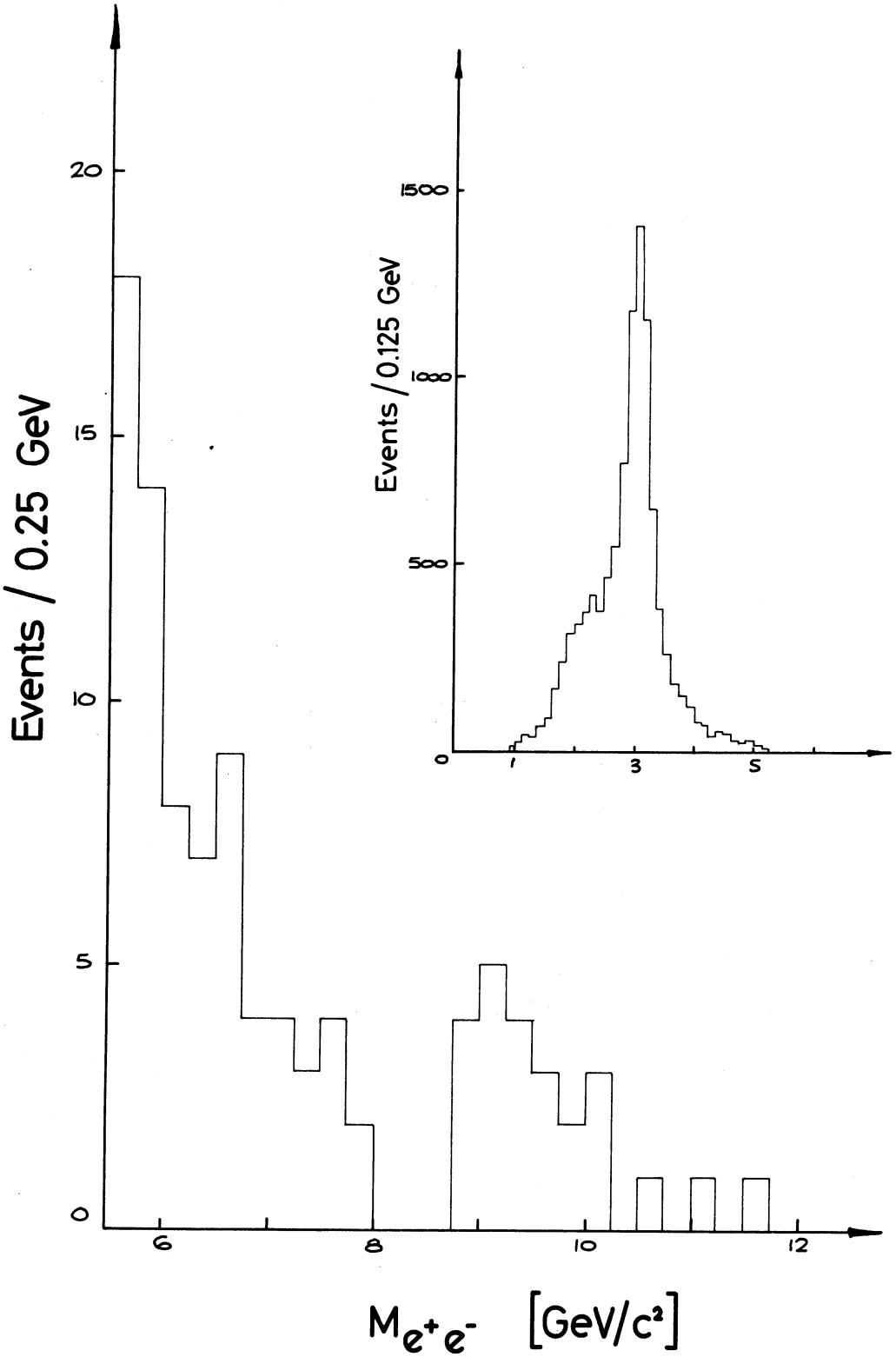
Events / 0.25 GeV
20
15
10
5
0
6
8
10
12
$M_{e^+e^-}$ [GeV/c²]
Events /0.125 GeV
1500
1000
500
0
1
3
5

Fig. 24